Challenge Journal of STRUCTURAL MECHANICS

Vol.1 No.1 (2015)

ISSN 2149-8024

TULPAR
ACADEMIC PUBLISHING

Challenge Journal of Structural Mechanics

E-mail: *cjsmec@challengejournal.com*

Web page: *cjsmec.challengejournal.com*

TULPAR Academic Publishing
www.tulparpublishing.com

Challenge Journal of Structural Mechanics

CONTENTS

TULPAR ACADEMIC PUBLISHING

Challenge Journal of Structural Mechanics

FRP-RC/PC members subjected to combined actions

A. Ghani Razaqpur [a], Francesco Bencardino [b], Lidia Rizzuti [b], Giuseppe Spadea [b,*]

[a] *Department of Civil Engineering, McMaster University, Hamilton, Ontario L8S 4L8, Canada*
[b] *Department of Civil Engineering, University of Calabria, V. P. Bucci, 87036 Rende (CS), Italy*

ABSTRACT

The capacity provisions of conventional Reinforced Concrete (RC) and Prestressed Concrete (PC) beams subjected to combined action of torsion, shear and flexure are well known and stated by international/national codes. Similar provisions lack for concrete members containing Fibre Reinforced Polymer (FRP) reinforcements. In general, there is paucity of research on the treatment of torsion combined with other stress resultants for FRP-RC/PC members. In this paper, the theoretical method proposed by the Canadian standard CSA S806 for FRP-RC/PC structures is presented. The critical issues, related to this topic, such as the appropriate strength and inclination of the diagonal struts and failure criteria are critically analyzed and addressed. In order to assess the reliability of this study a comparison between available experimental data regarding FRP-RC/PC beams subjected to combined actions and their corresponding theoretical provisions derived by the CSA S806 standard is shown. Furthermore, another approach, available in literature, which is based on the space truss model, is examined and used for comparison in order to evaluate the theoretical provisions offered by this model against the tests value of the set of the beams analyzed in this study. Based on the critical analysis of the results, it can be highlighted that the CSA method is able to conservatively predict the capacity of these beams.

ARTICLE INFO

Article history:
Received 4 January 2015
Accepted 17 February 2015

Keywords:
Combined actions
FRP bars/tendons
RC/PC members
Standards
Torsion

1. Introduction

Reinforced Concrete (RC) and Prestressed Concrete (PC) members can be subjected to torsion combined with other actions like shear and/or flexure. For conventional RC and PC structures, refined models have been developed to analyse the interaction of bending moment, shear force, and torsional moment. One of the early models developed on this topic is the one based on the skew-bending approach proposed by Elfgren et al. (1974), which is based on equilibrium considerations. It predicts the torsional capacity of the member without giving any indication about its deformations. Other semi-analytical and empirical models, some based on variable angle Space Truss Model (STM) of Rabbat and Collins (1978), or Compression Field Theory (CFT) of Collins and Mitchell (1997) and of Rahal (2007) have been developed for torsion combined with other actions. Further models proposed by Navarra-Gregori et al. (2007) and Swamy (1962) are available in literature. Some of these methods are included in concrete design codes such as the AASHTO LRDF (2012), the ACI 318 (2011), the CSA A23.3-04 (R2010), and the Eurocode (2004). The American Bridge Code AASHTO LRDF and the Canadian Standard CSA A23.3 include a design method based on the Modified Compression Field Theory (MCFT). This method, named as General Method (GM) (Collins et al., 1996; Rahan and Collins, 1999), accounts in a rational way how shear and torsion affect the stresses in the longitudinal steel located in the cross section. Similarly the procedure proposed by the ACI 318, is based on the thin-walled tube scheme and, space truss analogy. In all these three Code methods, the equations are suitable for designing sections subjected to shear, bending moment, axial load, and torsional moment. They are not suitable, however, for analysis of unsymmetrically reinforced sections if both flexural and torsional moments are acting.

* *Corresponding author*. Tel.: +39-0984-496919 ; Fax: +39-0984-496918 ; E-mail address: g.spadea@unical.it (G. Spadea)
ISSN: 2149-8024 / DOI: http://dx.doi.org/10.20528/cjsmec.2015.02.001

The use of Fibre Reinforced Polymer (FRP), as an alternative to conventional steel reinforcements in concrete members is on the rise, particularly when the long-term durability of reinforced concrete structures that are built in area with aggressive environment is the main concern. Indeed FRP reinforcements show advantageous properties, compared to conventional steel reinforcements, in terms of higher strength, durability, magnetic transparency, insulation, and lightweight. Nevertheless, FRP reinforcements have some shortcomings. In fact, unlike conventional steel bars FRP materials do not display plasticity and, exhibit very low shear strength, a lower elastic modulus. In general structures with FRP reinforcements are characterized by a clear lack of ductility. Based on these considerations, the design procedures developed for conventional RC or PC cannot be directly applied to FRP-RC/PC members. It has already been shown that new design methods are necessary for FRP RC sections subjected to shear and flexure (Ascione et al., 2010; Razaqpur and Spadea, 2014; Ascione et al., 2014). As a result, design codes and guidelines aimed at FRP-RC/PC structures ACI 440.1R (2006), ACI 440.4R (2004), CNR-DT 203 (2006), CSA S806 (2012), Fib 40 (2007), JSCE (1997) are available.

These guidelines, codes and standards give specific indications for bending and shear design while in some of them there is lack of specific provisions for the design of FRP-RC/PC members subjected to combined action of torsion, bending and shear. The latter may be partly due to the belief that torsion is regarded as secondary effect and not explicitly considered in design. In reality it is not always negligible and should be considered similar to other load effects, particularly if torsional moment is necessary for satisfying the equilibrium requirements. Actually, many structural elements such as spandrel beams, eccentrically loaded bridge girders, and beams curved in plan are subjected to the effects of combined actions. Moreover, there is a paucity of sufficient experimental and theoretical analysis about the behavior and the strength of FRP-RC/PC members.

However, if FRP reinforcement has to become a credible alternative to steel reinforcement, it is necessary that designers become familiar with suitable methods for designing FRP-RC/PC structures against any action and to their combination to which they may be subjected. As stated earlier, only few researches were developed by Probaghar and Kumaran (2011), Ragab and Eisa (2013) Razaqpur et al. (2011) about FRP-RC/PC members under pure torsion and by El-Awady et al. (2013) about FRP-RC members under combined torsion and flexure.

The new edition of the Canadian Standard CSA S806 furnishes detailed equations for the analysis and design of torsion combined with other stress resultants for FRP-RC/PC members. In this paper the background to the development of the provisions provided in the Canadian Standard is described, the key parameters that govern this topic are identified and discussed and the underlying arguments for the selection of the values of these parameters for FRP-RC/PC members are presented. The accuracy of the model proposed by the Canadian Standard is checked by comparing the predicted ultimate load of a number of FRP-RC/PC members involving carbon FRP (CFRP) and aramid FRP (AFRP) as both longitudinal and transverse reinforcement with the their corresponding experimental values. Admittedly, the amount of experimental is relatively limited, but for the purpose of the preceding comparison, all usable experimental data in the open literature are used. The recorded failure loads are also compared with the corresponding ultimate load computed by using Zhou's method (1997), which is an adaptation of the torsional design method in the Japanese Society of Civil Engineering (JSCE) concrete design standard.

It is important to emphasize at the outset that the focus of the current study is on the ultimate load, thus the statistical variability of the member material and geometric properties and their effect on ultimate loads are not germane to the study. When assessing a model's accuracy by comparing its predictions with experimental data from laboratory specimens, the specimens' material and geometric properties are known while statistical variability is reflected by the resistance factor which is obtained through reliability analysis. The results of the current study would provide the so-called model error for deriving the reliability-based resistance factor.

2. Theoretical Model and Basic Assumptions for RC and/or PC Members

As a prelude to the development of the design calculation procedure for FRP-RC/PC members subjected to combined actions, first the calculation method for conventional RC/PC members is briefly discussed. Design provisions for RC and PC beams subjected to combined torsion, shear and flexure actions assume that moment and axial forces acting on the cross section are resisted by normal stresses in the chords, while concomitant shear and torsion are resisted by shear flow in the walls of an equivalent hollow section. Due to different shear flows and the different strain conditions in the chords adjacent to the walls, the angle of inclination of the principal compressive stress, θ, will differ in each of the walls.

In the case of pure torsion, the diagonal stresses spirals around the member at a constant angle, while for zero torsion the diagonal stresses in the side walls are parallel. Furthermore, in the wall where shear stresses due to torsion and shear add, the angle θ is not greatly influenced by the loading ratio. In a solid section, it is normally assumed that the shear stresses due to the shear force are resisted by the solid section while the shear stresses due to torsion are resisted by the walls of an equivalent hollow section with wall thickness, t_w, and the area, A_{oh}, enclosed by the centerline of its walls. Thus, under the combined actions the longitudinal strains and the inclination θ, of the principal compressive stresses vary over the depth of the beam.

Theoretically, t_w is function of the angle of inclination of the struts θ, which in turn is function of the value of v/f_c and longitudinal strain ε_ℓ. With v the maximum shear stresses and f_c is the concrete compressive strength. The angle θ can be computed using strain compatibility and

equilibrium requirements, but the procedure is iterative. This circumstance is not convenient in design. Consequently, some code, suggest to put A_o=0.85A_{oh}, where A_{oh} and A_o are the areas enclosed by the centerlines of the hoops and the hollow tube, respectively, which allows one to determine t_w. To avoid iteration when designing a section against combined actions, the CSA A23.3 and AASHTO LRDF recommend that θ be calculated by using

$$\theta = 29 + 7000\varepsilon_l\,, \tag{1}$$

where θ is expressed in degrees. Here, the longitudinal strain ε_ℓ can be calculated by using the following expression

$$\varepsilon_l = \frac{\frac{M_n}{d_v}\sqrt{(V_n - V_p)^2 + \left(\frac{0.9p_h T_n}{2A_o}\right)^2} - A_p f_{po}}{2(E_l A_l + E_p A_p)}, \tag{2}$$

where M_n, V_n and T_n are the ultimate moment, shear strength and torsion at the section of interest (replaced by the factored moment, shear strength and torsion when designing), V_p is the component of the prestressing force at section opposing the applied shear force, d_v is the effective depth, taken as the greater of 0.9d or 0.72h, where d is the distance from the extreme compression fibre to the centroid of tension reinforcement and h is the overall height of the member, p_h is the length of the centerline of the hoop used as torsion reinforcement, A_p is the cross sectional area of the prestressed tendons, f_{po} is the effective stress in the prestressing tendons, A_l and A_p are the total area of non-prestressed and of prestressed longitudinal reinforcement in the cross-section respectively, E_l and E_p are the elastic moduli of non-prestressed and of prestressed longitudinal reinforcement in the tube cross-section.

Notice that Eqs. (1) and (2) allow one to compute θ as function of the rigidity of the longitudinal reinforcing and prestressing steel as well as the level of prestressing. Accordingly, one can adapt them for FRP-RC/PC members by inserting the appropriate axial rigidity of the FRP reinforcing/prestressing in Eq. (2) in lieu of that of steel. The substitution of steel rigidity by FRP rigidity is reasonable and the favourable agreement between the predicted and measured torsional strength values in this work indirectly supports the claim. However, more substantive support is provided by the work of Kanakubo and Shindo (1997).

On the side of the beam where the shear and torsional stresses are additive the shear stress can be evaluated, for solid section where significant redistribution of the shear stress is possible, by the following expression

$$v = \sqrt{\left(\frac{V_n - V_p}{bd_v}\right)^2 + \left(\frac{T_n}{1.7A_{oh}t_w}\right)^2}, \tag{3}$$

where b is the effective width of the section.

Once the tube dimensions and θ are known, the member nominal torsional, T_n, and shear strength, V_n, can be determined according to the Standard.

3. Application of the CSA Method to FRP-RC/PC Members

According to CSA S806, Eqs. (1) to (3) are applicable to FRP-RC/PC members with the following changes

(a) In Eq. (1) the constant 29 on the right-hand side is replaced by 30.

(b) In Eq. (2) the parameters E_l (E_p), A_l (A_p) for steel reinforcement (prestressing steel) are replaced by the corresponding properties of FRP reinforcing and prestressing bars, i.e. by E_F (E_{Fp}) and A_F (A_{Fp}), respectively.

(c) In Eq. (3) to avoid premature crushing of the diagonal struts the following limits should be satisfied

$$v \le 0.2f_c'\,. \tag{4}$$

The thickness t_w is assumed to be not greater than either the ratio A_{oh}/p_h or two times the minimum clear cover to the closed transverse torsion reinforcement.

(d) In the following equation to compute the torsional strength

$$T_n = 2A_o\frac{A_t f_{yt}}{s}\cot\theta\,, \tag{5}$$

the parameter A_t is replaced by the area of the FRP transverse reinforcement, A_{Ft}, and the yield strength of the transverse steel reinforcement, f_{yt}, are replaced by 0.4 f_{Fut}, where f_{Fut} is the ultimate or rupture strength of the transverse (hoops) FRP reinforcement used for torsion. It should be mentioned that f_{Fut} is the strength of a straight FRP bar with identical size and composition as the FRP hoop.

As stated before, FRP reinforcement differs from steel in a number of ways. FRP bars are transversely isotropic where the fibers are aligned along the longitudinal axis of the bar while steel is isotropic. FRP bars have a significantly higher strength and stiffness along the bar than perpendicular to the bar. FRP bars behave linear elastically up to failure and compared to steel bars they typically have much higher tensile strength, lower elastic modulus and lower ultimate strain. Therefore, in adapting the steel reinforced concrete designs methods to FRP, these characteristics of FRP and their effect on the strength of FRP reinforced members need to be recognized. It is important to point out that the fundamental space truss model that forms the basis of torsional strength equations in reinforced concrete design codes is independent of the reinforcement properties. The reinforcement properties affect the strength of the truss members and the inclination of its diagonal members, but not the truss model per se. This is the reason for the similarity of the equations used to determine the strength of FRP-RC/PC members with corresponding equations for steel reinforced members.

3.1. Analysis of FRP versus steel transverse reinforcement

When a reinforcing bar is bent in the shape of a stirrup or hoop, the axially stressed hoop will be subjected to radial compressive stress in its corner. The magnitude of this stress depends on the ratio r_b/d_b and the magnitude

of the axial stress in the bar, where r_b is the radius of the bend and d_b is the diameter of the bar. The radial stress (σ_r) combined with the axial stress (σ_l) in the bar creates a state of biaxial stress at the bent corner. The radial stress is generally smaller than the axial stress; therefore, in the case of steel rebar, which are isotropic and ductile, the effect of radial stress is relatively small and it can be safely ignored. In the case of FRP bars, due to the smaller strength and modulus of the bar in the radial than the longitudinal (circumferential) direction and the biaxial tensile-compressive state of the stress at the bend, the bent bar fails at a lower axial load than a similar straight bar. The failure envelope for this biaxial state of stress is theoretically not only function of the geometric parameter r_b/d_b, but also of the fiber and resin type and the bar fiber content. In the ACI 440 and in the JSCE guideline an equation is proposed to evaluate the tensile strength of the FRP bent bar. The CSA S806 adopted a safe limit for design by analyzing the results of the formula proposed by the ACI guideline against the experimental data available in literature. It is recognized that this assumption may yield a conservative estimate of the nominal torsional strength of FRP-RC/PC members, but is practically more convenient because it does not require knowledge of the hoop bend angle at the design stage.

3.2. Diagonal cracks angle, θ

An important parameter that need be determined is the angle θ, which can be calculated using Eq. (1). Since θ is given as function of the longitudinal reinforcement rigidity, it can be calculated if in Eq. (2) the steel elastic modulus, E_l (E_p), is replaced by the corresponding FRP elastic modulus, E_F (E_{Fp}). The angle θ is known to vary depending on the beam properties and for this reason the ACI 318 allows any value of θ between 30° and 60°, but suggests θ be taken as 45° for reinforced concrete members and 37.5° for prestressed concrete members. While selecting a suitable angle when designing a steel reinforced member for torsion is justifiable because equilibrium requirements can be satisfied for any reasonable value of θ, assessing the strength of existing members requires more accurate calculation of the angle θ, for neither θ = 45° nor any other arbitrarily fixed value is likely to give an accurate estimate of the actual strength of every member. In the case of FRP reinforced members, the assumption of θ = 45° may not be appropriate even for design purposes, especially for calculating the amount of transverse reinforcement, because such an assumption treats all types of FRP reinforcement the same, irrespective of the substantial differences that exists among the mechanical properties of different types of FRP. There would be little theoretical justification for such an assumption and in certain cases it could lead to a substantial overestimation of the strength of a member.

Since Eq. (1) for computing θ accounts for the effect of the axial rigidity of the longitudinal reinforcement on the inclination of the diagonal cracks, the CSA S806 recommends this equation for computing θ to be used, but following both the ACI 318 and CSA A23.3, it also stipulates that θ may not be taken less than 30° nor greater than 60°.

4. Zhou's Model

The Zhou's model is based on the method of Kojima et al. (1997) and is similar to the pre-1998 ACI code approach and is only applicable to PC members. In this model T_n can be calculated by summing the contribution of the concrete, T_{nc}, and the contribution of the reinforcement, T_{ns} to the torsional resistance as

$$T_n = T_{nc} + T_{ns}\,. \tag{6}$$

According to this model the torsional failure of a FRP-RC/PC member may be initiated by rupture of transverse or longitudinal reinforcement, and torsional strength is reached whichever occurs first. Zhou adopted this method but introduced a modification factor that takes into account the difference between the FRP and steel mechanical properties. T_{nc} can be calculated by using

$$T_{nc} = \gamma k\left(1-2\tfrac{t_w}{b}\right)^2\left(1-2\tfrac{t_w}{b}\right)\,,\quad \gamma = \sqrt{1+\tfrac{\sigma_p}{f_t}}\,, \tag{7}$$

where b is the member width, f_t is the tensile strength of concrete, γ is the factor that take into account the effective prestress, σ_p is the effective prestress.

k is given by:

$$k = T_{te} + 0.25\left(T_{tp}-T_{te}\right)\left(\tfrac{f_b}{f_t}-1\right)\left(5-\tfrac{f_b}{f_t}\right), \tag{8}$$

where f_b is the modulus of rupture of concrete.

T_{te} and T_{tp} are computed using:

$$T_{te} = b^2 h f_t \tfrac{1}{3+1.8\frac{b}{h}}\,, \tag{9}$$

where h is the overall height of the member.

$$T_{te} = 0.5 b^2 h f_t\left(1-\tfrac{b}{3h}\right). \tag{10}$$

The torsional resistance provided by transverse reinforcement, T_{nts}, is calculated using

$$T_{nts} = 2A_{oh}\tfrac{A_{Ft} f_{Fut}}{\gamma s}\sqrt{\tfrac{E_{Ft}}{E_s}}. \tag{11}$$

The torsional resistance provided by the longitudinal reinforcement, T_{nls}, is computed as

$$T_{nls} = 2A_{oh}\tfrac{A_{Ft} f_{Ful}}{\gamma P_h}\sqrt{\tfrac{E_F}{E_s}} + 2A_{oh}\tfrac{\sigma_p t_w}{\gamma}\,, \tag{12}$$

where E_s is the modulus of elasticity of steel (200 GPa), E_{Ft} is the modulus of elasticity of the transverse reinforcements, f_{Ful} is the ultimate strengths of the FRP longitudinal reinforcement, f_{Fut} is the ultimate strengths of the FRP transverse reinforcement.

Note that the angle θ is not directly considered in these equations, but is assumed to be equal to 45°.

According to Zhou's model in the case of combined torsion and bending actions it is possible to use the Swamy formula:

$$\left(\frac{T_n}{T_0}\right)^2 + \left(\frac{M_n}{M_0}\right)^2 = 1\,, \tag{13}$$

where T_n and M_n are the torsional and the ultimate bending strength, respectively and T_0 and M_0 are the pure torsional and pure bending ultimate strength of the section, respectively.

5. Collection of Experimental Data

Experimental data of FRP-RC and FRP-PC beams subjected to combined torsion, shear and flexure, available in literature (Zhou, 1997; Yonekura et al., 1994), were analysed and collected in a database. The relevant geometric and material properties of the beams are given in Table 1. The details of the mechanical properties with the experimental results are given in Table 2. In all these tests, the beams had a rectangular cross section. The internal reinforcements used were either CFRP or AyFRP bars.

Table 1. Geometric data and material properties of FRP-RC/PC beams tested under combined actions.

Data source	Specimen name	Geometric data		Concrete	Prestress	Load	FRP longitudinal reinforcement			
		b (mm)	h (mm)	f_c (MPa)	σ_P (MPa)	T/M	Type	A_l (mm²)	f_l (MPa)	E_l (GPa)
Zhou (1997) & Yonekura et al. (1994)	A1	140	220	49.0	-	0.3	AFRP	172.0	1860	53
	A2	140	220	49.0	12.24	0.3	AFRP	172.0	1860	53
	A3	140	220	49.0	11.28	0.3	AFRP	172.0	1860	53
	A4	140	220	49.0	11.19	0.3	AFRP	172.0	1860	53
	A5	140	220	49.0	11.68	0.3	AFRP	516.0	1860	53
	A6	140	220	49.0	11.92	1.2	AFRP	172.0	1860	53
	A7	140	220	78.0	11.77	1.2	AFRP	172.0	1860	53
	A8	140	220	49.0	11.49	1.2	AFRP	516.0	1860	53
Zhou (1997) & Yonekura et al. (1994)	C1	140	220	49.0	-	0.3	CFRP	201.2	2110	136
	C2	140	220	49.0	-	0.3	CFRP	839.6	1910	129
	C3	140	220	49.0	9.17	0.3	CFRP	201.2	2110	136
	C4	140	220	49.0	12.23	0.3	CFRP	201.2	2110	136
	C5	140	220	49.0	12.32	0.3	CFRP	201.2	2110	136
	C6	140	220	49.0	12.32	0.3	CFRP	839.6	1910	129
	C7	140	220	49.0	9.10	1.2	CFRP	201.2	2110	136
	C8	140	220	49.0	12.40	1.2	CFRP	201.2	2110	136
	C9	140	220	49.0	-	1.2	CFRP	201.2	2110	136
	C10	140	220	49.0	12.38	1.2	CFRP	201.2	2110	136
	C11	140	220	49.0	11.52	1.2	CFRP	201.2	2110	136
	C12	140	220	78.0	11.77	1.2	CFRP	201.2	2110	136
	C13	140	220	49.0	12.76	1.2	CFRP	839.6	1910	129

Note: b=member width; h=member overall height; f_c'=concrete cylinder compressive strength; σ_P=effective prestress; T=torsional moment; M=bending moment; A_l, f_l, E_l=area, ultimate strength, and elasticity modulus of longitudinal reinforcements.

6. Comparison of the Theoretical Previsions Against Experimental Data

In Table 3, for the beams listed in Table 1 and in Table 2, the experimental failure load, P_{exp}, and its corresponding theoretical value, P_{th}, computed according the two methods analyzed are given for each beam. For the CSA S806 method the angle of inclination θ is shown in the table, while it's omitted for the Zhou's model since it is assume θ=45°. Moreover, for all the beams the mean value of the ratio P_{exp}/P_{th}, its standard deviation and coefficient of variation are also given. When calculating the ultimate capacity of each beam by either method, the material resistance factors were set equal to one. In the case of the Zhou's model the mean value of the ratio P_{exp}/P_{th} is 0.95, with a standard deviation of 0.33 while the corresponding values for the CSA method are 1.12 and 0.22. It can be noticed that this model overestimates the capacity of the RC beams, while the capacity of PC beams is underestimated by over 50% in some cases. The Canadian Standard generally predicts the strength of the same beams more accurately, but it seems to overestimate the capacity of the RC beams with high amount of longitudinal reinforcement. On the whole, the method gives rea-

sonable results for both the AFRP and the CFRP reinforced and prestressed beams. Therefore, the design strength of all the beams according to CSA S806 would be on the safe side, even if other relevant statistical variables were factored in (Fig. 1(a)). While in the case of the Zhou's model some of the beam are on the unsafe side (Fig. 1(b)).

Table 2. Mechanical properties and experimental results of FRP-PC and FRP-RC beams tested under combined actions.

Data source	Specimen name	FRP transverse reinforcement					P_{exp} (kN)	T_{exp} (kNm)	M_{exp} (kNm)	V_{exp} (kN)
		Type	A_t (mm²)	f_t (MPa)	E_t (GPa)	s (mm)				
Zhou (1997) & Yonekura et al. (1994)	A1	AFRP	28.3	1860	53	70	67	4.82	16.07	33
	A2	AFRP	28.3	1860	53	70	113	8.13	27.10	56
	A3	AFRP	28.3	1860	53	40	121	8.73	29.10	61
	A4	AFRP	12.6	1860	53	40	110	7.89	26.30	55
	A5	AFRP	28.3	1860	53	70	109	7.86	26.20	55
	A6	AFRP	28.3	1860	53	70	30	8.67	7.23	15
	A7	AFRP	28.3	1860	53	70	38	10.85	9.04	19
	A8	AFRP	28.3	1860	53	70	29	8.38	6.98	15
Zhou (1997) & Yonekura et al. (1994)	C1	CFRP	28.3	1670	118	110	63	4.50	15.00	31
	C2	CFRP	28.3	1670	118	110	77	5.56	18.53	39
	C3	CFRP	28.3	1670	118	110	101	7.26	24.20	50
	C4	CFRP	28.3	1670	118	110	125	9.02	30.07	63
	C5	CFRP	28.3	1670	118	110	117	8.40	28.00	58
	C6	CFRP	28.3	1670	118	110	111	7.96	26.53	55
	C7	CFRP	28.3	1670	118	110	29	8.38	6.98	15
	C8	CFRP	28.3	1670	118	110	33	9.61	8.01	17
	C9	CFRP	28.3	1670	118	110	19	5.42	4.52	9
	C10	CFRP	28.3	1670	118	110	34	9.84	8.20	17
	C11	CFRP	28.3	1670	118	40	43	12.24	10.20	21
	C12	CFRP	28.3	1670	118	40	45	13.02	10.85	23
	C13	CFRP	28.3	1670	118	110	31	8.94	7.45	16

Note: A_t, f_t, E_t=area, ultimate strength, and modulus of elasticity of transversal reinforcements; s=transversal reinforcements spacing; P_{exp}=load attained at failure; T_{exp}, M_{exp}, V_{exp}=failure torsional moment, bending moment, shear force, measured in the test.

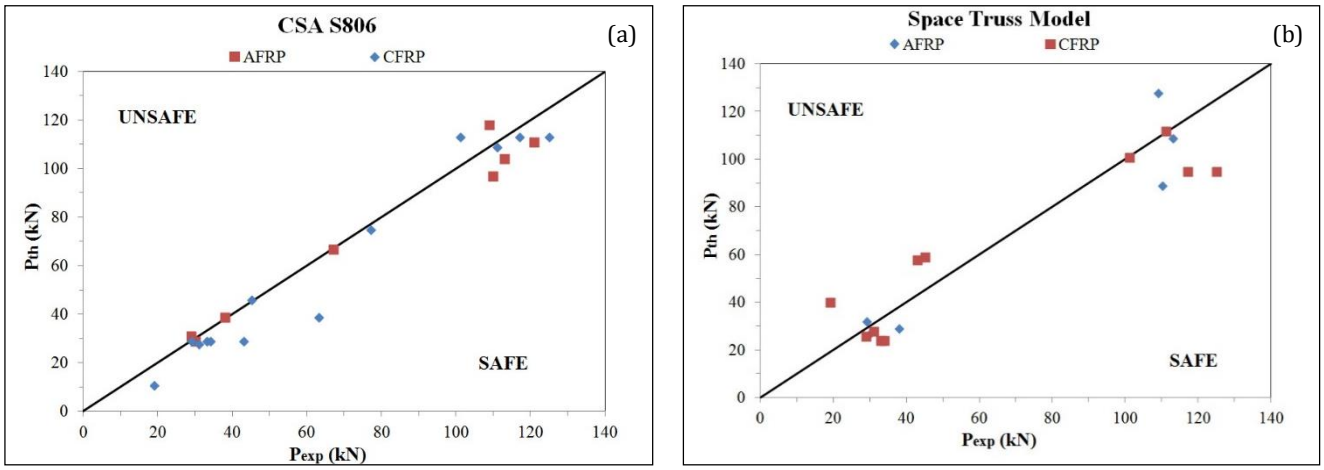

Fig. 1. Comparison of experimental data with theoretical provisions: a) CSA S806, b) Space truss model.

Table 3. Comparison between theoretical and experimental failure loads.

Data source	Specimen name	P_{exp} (kN)	CSA S806			Zhou	
			P_{th} (kN)	P_{exp}/P_{th}	θ (°)	P_{th} (kN)	P_{exp}/P_{th}
Zhou (1997) & Yonekura et al. (1994)	A1	67	67	1.00	60	150	0.45
	A2	113	104	1.09	48	109	1.04
	A3	121	111	1.09	60*	171	0.71
	A4	110	97	1.13	42	89	1.24
	A5	109	118	0.92	50*	128	0.85
	A6	30	29	1.03	37*	27	1.11
	A7	38	39	0.97	37	29	1.31
	A8	29	31	0.94	52*	32	0.91
Zhou (1997) & Yonekura et al. (1994)	C1	63	39	1.62	60	161	0.39
	C2	77	75	1.03	49	203	0.38
	C3	101	113	0.89	30*	101	1.00
	C4	125	113	1.11	30*	95	1.32
	C5	117	113	1.04	30*	95	1.23
	C6	111	109	1.02	33*	112	0.99
	C7	29	29	1.00	30	26	1.12
	C8	33	29	1.14	30	24	1.38
	C9	19	11	1.73	56	40	0.48
	C10	34	29	1.17	30	24	1.42
	C11	43	29	1.48	36*	58	0.74
	C12	45	46	0.98	30*	59	0.76
	C13	31	28	1.11	30*	28	1.11
	Mean			*1.12*			*0.95*
	Standard deviation			*0.22*			*0.33*
	Coefficient of variation			*0.20*			*0.35*

* failure governed by concrete crushing

7. Conclusions

The following main conclusions can be drawn from this study:

- The capacity of FRP reinforced and prestressed concrete members under combined action of flexure, shear and torsion can be accurately determined by using the proposed design provisions of the Canadian Standard CSA S806.
- With reference to the Canadian Standard, the mean value of the ratio of the experimental to theoretical strength ratio is 1.12, with a standard deviation of 0.22.
- The mean value of experimental to theoretical strength based ratio based on the space truss model is 0.95, with a standard deviation of 0.33. Furthermore, the method underestimates the strength of many beams, some by over 50%. Accordingly, this method requires further improvement before it can be used in design.
- Additional test data involving a wider range of shear, torsion and flexure ratios, in addition to the internal reinforcement amount and arrangement, are needed to fully validate the proposed CSA S806 method and its reliability.

References

AASHTO LRFD (2012). Bridge Design Specifications. American Association of State Highway and Transportation Official, Washington, DC.

Ascione L, Mancusi G, Spadea S (2010). Flexural behaviour of concrete beams reinforced with GFRP bars. *Strain*, 46(5), 460-469.

Ascione L, Razaqpur AG, Spadea S (2014). Effectiveness of FRP stirrups in concrete beams subject to shear. *Proceedings of the 7th International Conference on FRP Composites in Civil Engineering (CICE 2014)*.

ACI 440.1R (2006). Guide for the design and construction of structural concrete reinforced with FRP bars. American Concrete Institute, Farmington Hills, MI.

ACI 440.4R (2004). Prestressed concrete structures with FRP tendons. American Concrete Institute, Farmington Hills, MI.

ACI 318 (2011). Building code requirements for structural concrete and commentary. American Concrete Institute, Farmington Hills, MI.

CNR-DT 203 (2006). Guide for the design and construction of concrete structures reinforced with fiber-reinforced polymer bars. National Research Council CNR, Rome, Italy.

CSA A23.3 (2004) (Reaffirmed 2010). Design of concrete structures. Canadian Standards Association, Rexdale, Ontario, Canada.

CSA S806 (2012). Design and construction of building components with fibre-reinforced polymers. Canadian Standards Association, Rexdale, Ontario, Canada.

Collins MP, Mitchell D (1997). Prestressed Concrete Structures. Response Publication, Canada.

Collins MP, Mitchell D, Adebar PE, Vecchio FJ (1996). A general shear design method. *ACI Structural Journal*, 93(1), 36-45.

El-Awady E, Husain M, Mandour S (2013). FRP-Reinforced concrete beams under combined torsion and flexure. *International Journal of Engineering Science and Innovative Technology*, 2(1), 384-393.

Elfgren L, Karlsson I, Losberg A (1974). Torsion-bending-shear interaction for concrete beams. *Journal of Structural Division*, 100(8), 1657–1676.

Eurocode 2 (2004). Design of concrete structures – Part 1-1: general rules and rules for buildings. EN 1992-1-1:2004, European Committee for Standardization.

Fib 40 (2007). FRP reinforcement in RC structures. International Federation for Structural Concrete.

JSCE (1997). Recommendation for design and construction of concrete structures using continuous fiber reinforcing materials. Concrete Engineering, Series 23.

Kanakubo T, Shindo M (1997). Shear behavior of fiber-mesh reinforced plates. *Proceedings of the 3rd International Symposium on Non-Metallic (FRP) Reinforcement for Concrete Structures – International Symposium*, Sapporo, Japan, October, 2, 317-324.

Kojima T, Takagi N, Uegaki Y (1991). Study on ultimate torque of prestressed reinforced concrete beams with large section subjected to pure torsion. *Transaction of the Japan Concrete Institute*, 13, 553-560.

Navarro-Gregori J, Miguel-Sosa P, Fernandez-Prada MA, Filippou FC (2007). A 3D numerical model for reinforced and prestressed concrete elements subjected to combined axial, bending, shear and torsion loading. *Engineering Structures*, 29, 3404-3419.

Prabaghar A, Kumaran G (2011). Theoretical study on the behaviour of rectangular concrete beams reinforced internally with GFRP reinforcements under pure torsion. *International Journal of Civil and Structural Engineering*, 2(2), 570-594.

Rabbat B, Collins MP (1978). A variable angle space truss model for structural concrete members subjected to complex loading. In: *International Symposium on Concrete and Concrete Structures*. SP-55. Detroit: American Concrete Institute, 547-587.

Ragab KS, Eisa AS (2013). Torsion behaviour of steel fibered high strength self compacting concrete beams reinforced by GFRP bars. *International Journal of Civil Science and Engineering,* 7(9), 218-228.

Rahal KN (2007). Combined torsion and bending in reinforced and prestressed concrete beams using simplified method for combined stress-resultants. *ACI Structural Journal,* 104(4), 402-411.

Rahal KN, Collins MP (1999). Background of the general method of shear design in the 1994 CSA-A23.3 Standard. *Canadian Journal of Civil Engineering*, 26(6), 827-839.

Razaqpur AG, Rizzuti L, Bencardino F, Spadea G (2011). FRP-PC members: evaluation of torsional capacity. In *ACIC 2011 conference on advanced composites in construction*, Warwick, UK, 6-8 September, 319-328.

Razaqpur AG, Spadea S (2014). Shear strength of FRP reinforced concrete members with stirrups. *Journal of Composites for Construction*, 19(1).

Swamy RN (1962). The behavior and ultimate strength of prestressed concrete hollow beams under combined bending and torsion. *Magazine of Concrete Research*, 14(40), 13-24.

Zhou P (1997). Mechanical characteristics of prestressed concrete beams and columns with fiber reinforced plastics. Report, University of Hiroshima, Japan.

Yonekura A, Tazawa E, Zhou P, Sumi H (1994). Mechanical behavior of prestressed concrete beams with FRP rods subjected to combined bending and torsional moments. *Transaction of the Japan Concrete Institute*, 16, 217-224.

Challenge Journal of Structural Mechanics

Parametric analysis of thick plates subjected to earthquake excitations

Yaprak Itır Özdemir [a], Yusuf Ayvaz [b,*], Tayfun Dede [a]

[a] *Department of Civil Engineering, Karadeniz Technical University, 61080 Trabzon, Turkey*
[b] *Department of Civil Engineering, Yıldız Technical University, 34220 İstanbul, Turkey*

ABSTRACT

Plates are structural elements commonly used in the building industry. A plate is considered to be a thin plate if the ratio of the plate thickness to the smaller span length is less than 1/20; it is considered to be a thick plate if this ratio is larger than 1/20. The purpose of this paper is to study shear locking-free analysis of thick plates using Mindlin's theory and to determine the effects of the thickness/span ratio, the aspect ratio and the boundary conditions on the linear responses of thick plates subjected to earthquake excitations. Finite element formulation of the equations of the thick plate theory is derived by using second order displacement shape functions. A computer program using finite element method is coded in C++ to analyze the plates clamped or simply supported along all four edges. In the analysis, 17-noded finite element is used. Graphs and tables are presented that should help engineers in the design of thick plates subjected to earthquake excitations.

ARTICLE INFO

Article history:
Received 26 December 2014
Accepted 7 March 2015

Keywords:
Shear locking-free analysis
Earthquake
Thick plate
Mindlin's theory
Finite element method

1. Introduction

In the past 30 years, using of the plate bending elements based on the Mindlin (1951), and Reissner (1947) theory (the first-order shear deformation theory) have interested many researchers. Numerous methods have been proposed by earlier researchers for solving plate bending problem. In Mindlin-Reissner plate theory formulation's the deflection w and rotations βx, βy are generally considered to be independent function therefore only C0-continuity is required. The most encountered phenomenon is shear locking which acts as the plate becomes incrementally thinner.

In order to avoid this problem, the method of reduced and selective reduced integration (Zienkiewicz et al., 1971; Hughes et al., 1977; Ozkul and Ture, 2004) are chosen instead of the full integration, the substitute shear strain method proposed by Hinton et al, (1986), free formulation method proposed by Bergan et al. (1984). The same problem can also be prevented by using higher order displacement shape function (Özdemir et al., 2007). This paper that improved element is used for the vibration analysis of the plate.

The aim of this paper is to study forced vibration analysis of thick plates using Mindlin's theory and to determine the effects of the thickness/span ratio, the aspect ratio and the boundary conditions on the linear responses of thick plates subjected to earthquake excitations.

A computer program using finite element method is coded in C++ to analyze the plates clamped or simply supported along all four edges. In the program, the finite element method is used for spatial integration and the Newmark-β method is used for time integration. In the analysis, 17-noded finite elements are used to construct the stiffness and mass matrices.

2. Finite Element Modeling

The governing equation for a flexural plate subjected to an earthquake excitation without damping can be given as

$$[M]\{\ddot{w}\} + [K]\{w\} = [F] = -[M]\{\ddot{u}_g\}, \quad (1)$$

* *Corresponding author*. Tel.: +90-212-3835213 ; Fax: +90-212-3835213 ; E-mail address: yayvaz@yildiz.edu.tr (Y. Ayvaz)
ISSN: 2149-8024 / DOI: http://dx.doi.org/10.20528/cjsmec.2015.03.002

where [K] and [M] are the stiffness matrix and the mass matrix of the plate, respectively, w and $\ddot{w}$ are the lateral displacement and the second derivative of the lateral displacement of the plate with respect to time, respectively; and $\ddot{u}_g$ is the earthquake acceleration.

In order to do forced vibration analysis of a plate, the stiffness, [K], mass matrices, [M], and equivalent nodal loads vector, [F], of the plate should be constructed. The evaluation of these matrices is given in the following sections.

2.1. Evaluation of the stiffness matrix

In this study, 17-noded quadrilateral serendipity element (MT17) (Fig. 1) is used. The stiffness matrix for this element can be obtained by the following equation (Cook et al., 1989; Özdemir et al., 2007),

$$K = \int_A [B]^T [D][B] dA = \int_{-1}^{1}\int_{-1}^{1} B^T D B\, |J| dr ds\,, \qquad (2)$$

which must be evaluated numerically (Weaver and Jahston, 1984).

As seen from Eq. (2), in order to obtain the stiffness matrix, the strain–displacement matrix, [B], and the flexural rigidity matrix, [D], of the element need to be constructed and can be seen Özdemir and Ayvaz (2007).

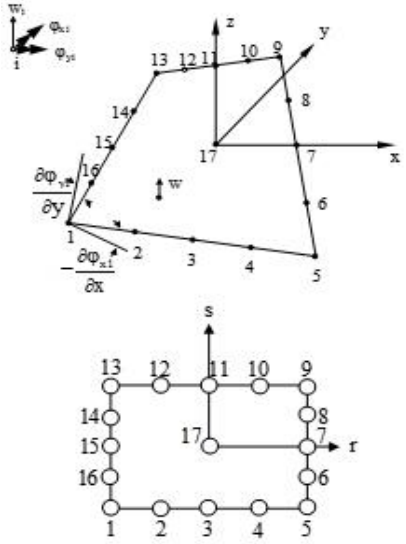

Fig. 1. 17-noded quadrilateral finite element used in this study.

2.2. Evaluation of the mass matrix

The formula for the consistent mass matrix of the plate may be written as

$$M = \int_\Omega H_i^T \mu H_i \, d\Omega\,. \qquad (3)$$

In this equation, μ is the mass density matrix of the plate (Özdemir et al., 2007) and H_i can be written as follows,

$$H_i = [dh_i/dx \quad dh_i/dy \quad h_i] \quad i = 1, \ldots, 17\,. \qquad (4)$$

It should be noted that the rotation inertia terms are not taken into account. By assembling the element mass matrices obtained, the system mass matrix is obtained.

2.3. Evaluation of equivalent nodal loads vector

Equivalent nodal loads, [F], can be obtained by the following equation.

$$[F] = \int H_i^T \bar{q} d\Omega\,. \qquad (5)$$

In this equation, H_i can be obtained by Eq. (4), and $\bar{q}$ denotes;

$$\bar{q} = -[M]\{\ddot{u}_g\}\,. \qquad (6)$$

It should be noted that, the Newmark-β method is used for the time integration of Eq. (1) by using the average acceleration method.

3. Numerical Examples

3.1. Data for numerical examples

In the light of the results given in references (Özdemir and Ayvaz, 2007), the aspect ratios, b/a, of the plate are taken to be 1, 1.5, 2.0, and 3.0. The thickness/span ratios, t/a are taken as 0.05, 0.1, 0.2, and 0.3 for each aspect ratio. The shorter span length of the plate is kept constant to be 3 m. The mass density, Poisson's ratio, and the modulus of elasticity of the plate are taken to be 2.5 kN/m^2, 0.2, and 2.8x10^7 kN/m^2 for both analysis. In order to obtain the response of each plate in the analysis, the first 8 s of the East-West component of the March 13, 1992 Erzincan earthquake in Turkey is used since the peak value of the record occurred in this range.

For the sake of accuracy in the results, rather than starting with a set of a finite element mesh size and time increment, the mesh size and time increment required to obtain the desired accuracy were determined before presenting any results. This analysis was performed separately for the mesh size and time increment. It was concluded that the results have acceptable error when equally spaced 4x4 mesh sizes are used for a 3 m x 3 m plate, if the 0.01 s time increment is used. Length of the elements in the x and y directions are kept constant for different aspect ratios as in the case of square plate.

3.2. Results

The absolute maximum values of displacements and bending moments of the plates modeled using MT17 element for different aspect ratios are presented in this study. The absolute maximum displacements of the plates for different aspect ratios, and thickness/span ratios are given in Fig. 2.

The absolute maximum bending moments M_x and M_y at the center of the plates simply supported and clamped plates along all four edges for different aspect ratios, and thickness/span ratios are given in Figs. 3 and 4, respectively.

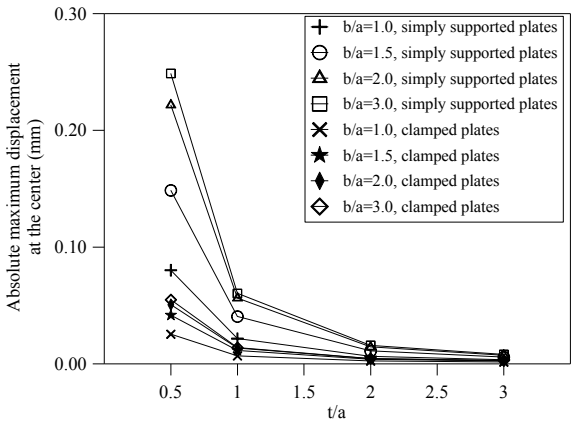

Fig. 2. Absolute maximum displacement of the simply supported and clamped plates for different aspect ratios and thickness/span ratios.

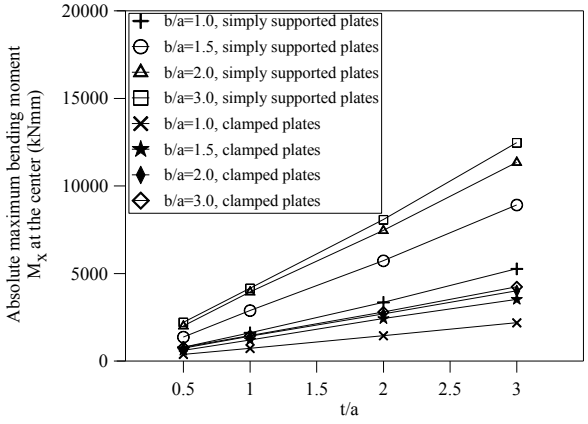

Fig. 3. Absolute maximum bending moment M_x at the center of the simply supported and clamped plates for different aspect ratios and thickness/span ratios.

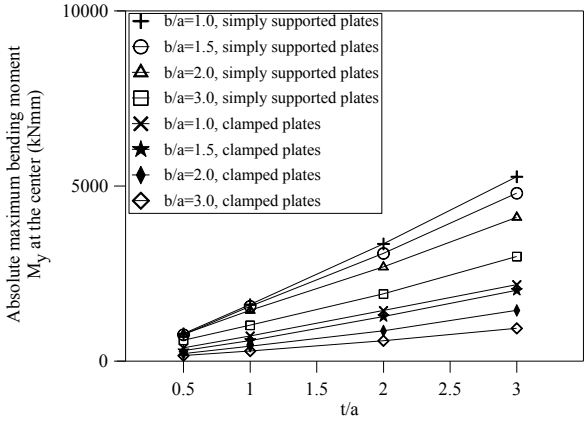

Fig. 4. Absolute maximum bending moment M_y at the center of the simply supported and clamped plates for different aspect ratios and thickness/span ratios.

As seen from Fig. 3, the absolute maximum bending moments M_x at the center of simply supported and clamped plates increase with increasing aspect ratio and thickness/span ratio. The increase in the maximum bending moment M_x decreases with increasing aspect ratio, and increases with increasing thickness/span ratio. In general, the effects of the changes in the aspect ratios on the absolute maximum bending moment, M_x, are larger than the changes in the thickness/span ratios.

As seen from Fig. 4, the absolute maximum bending moments M_y at the center of simply supported and clamped plates decreases with increasing aspect ratio and thickness/span ratio. The decrease in the maximum bending moment M_y increases with increasing aspect ratio, and decreases with decreasing thickness/span ratio. In general, the effects of the changes in the thickness/span ratios on the absolute maximum bending moment, M_y, are larger than the changes in the aspect ratios.

In this study, the absolute maximum bending moments M_x at the center of the edge in the y direction and the maximum bending moment M_y at the center of the edge in the x direction are not presented for the thick plates clamped along all four edges. It should be noted that the variations of these moments are similar to the absolute maximum bending moments M_x at the center of the thick clamped plates.

The effectiveness of the aspect and thickness/span ratios on the maximum responses considered in this study depends on the values of them. But, in general, the thickness/span ratio is more effective on the maximum responses than the aspect ratio.

4. Conclusions

The purpose of this paper was to study shear locking-free analysis of thick plates using Mindlin's theory by using 17-noded finite elements and to determine the effects of the thickness/span ratio, the aspect ratio and the boundary conditions on the maximum displacements and bending moments of thick plates subjected to earthquake excitations. It is concluded that the coded program can effectively be used in the earthquake analysis of the thick plates by using 17-noded finite element. The following conclusions can also be drawn from the results obtained in this study.

The absolute maximum displacements of the thick plates increase with increasing aspect ratio for a constant t/a ratio. The same displacements decrease with increasing t/a ratio for a constant b/a ratio. The effects of the changes in the thickness/span ratios on the absolute maximum displacement are generally larger than the changes in the aspect ratios.

The absolute maximum bending moment, M_x, at the center of the thick simply supported and clamped plates increases with increasing aspect ratio and thickness/span ratio. The effects of the changes in the aspect ratios on the absolute maximum bending moment, M_x, of the thick simply supported and clamped plates are generally larger than the changes in the thickness/span ratios.

The absolute maximum bending moment, M_y, at the center of the thick simply supported and clamped plates decreases with increasing aspect ratio and increases with increasing thickness/span ratio. The effects of the changes in the thickness/span ratios on the absolute maximum bending moment, M_y, of the thick simply supported and clamped plates are generally larger than the

changes in the aspect ratios. The effectiveness of the aspect and thickness/span ratios on the maximum responses considered in this study depends on the values of them.

In general, degrees of decreases and increases depend on the changes in the aspect and thickness/span ratios, and the changes in the thickness/span ratio are more effective on the maximum responses considered in this study than the changes in the aspect ratio.

REFERENCES

Ayvaz Y (1992). Parametric Analysis of Reinforced Concrete Slabs Subjected to Earthquake Excitation. *Ph.D. thesis*, Graduate School of Texas Tech University, Lubbock, Texas.

Bathe KJ (1996). Finite Element Procedures. Prentice Hall, Upper Saddle River, New Jersey.

Bergan PG, Wang X (1984). Quadrilateral plate bending elements with shear deformations. *Computer and Structures*, 19(1-2), 25-34.

Cook RD, Malkus DS, Michael EP (1989). Concepts and Applications of Finite Element Analysis. John Wiley & Sons, Inc., Canada.

Hinton E, Huang HC (1986). A family of quadrilateral Mindlin plate element with substitute shear strain fields. *Computers and Structures*, 23(3), 409-431.

Hughes TJR, Taylor RL, Kalcjai W (1977). A simple and efficient element for plate bending. *International Journal for Numerical Methods in Engineering*, 11(10), 1529-1543.

Mindlin RD (1951). Influence of rotatory inertia and shear on flexural motions of isotropic, elastic plates. *Journal of Applied Mechanics*, 18, 31-38.

Ozkul TA, Ture U (2004). The transition from thin plates to moderately thick plates by using finite element analysis and the shear locking problem. *Thin-Walled Structures*, 42, 1405-1430.

Özdemir YI, Bekiroğlu S, Ayvaz Y (2007). Shear locking-free analysis of thick plates using Mindlin's theory. *Structural Engineering and Mechanics*, 27(3), 311-331.

Özdemir YI, Ayvaz Y (2007). Shear locking-free analysis of thick plates subjected to earthquake excitations. *International Conference on Civil, Structural and Environmental Engineering Computing*, St. Julians, Malta, September 18-21, 212-227.

Reissner E (1947). On bending of elastic plates. *Quarterly of Applied Mathematics*, 5, 55-68.

Weaver W, Johnston PR (1984). Finite Elements for Structural Analysis. Prentice Hall Inc., Englewood Cliffs, New Jersey.

Zienkiewich OC, Taylor RL, Too JM (1971). Reduced integration technique in general analysis of plates and shells. *International Journal for Numerical Methods in Engineering*, 3, 275-290.

Challenge Journal of Structural Mechanics

An experimental study on influence of shear failure type partial wall on reinforced concrete frame

Hisato Hotta *, Takeshi Nakajima

Department of Architecture and Building Engineering, Tokyo Institute of Technology, 152-8550 Tokyo, Japan

ABSTRACT

Partial walls separated from columns are generally treated as nonstructural elements because their behavior aren't analyzed much. Partial walls jointed rigidly to RC frames raise horizontal load-carrying capacity, however they may give an influence on RC frames when they fall in brittle failure. Objective of this paper is to clarify the influence of partial walls falling in shear failure on RC frames through a static loading test and a shaking table test. The experiment shows that, after one of the partial walls fails, story drift rapidly increases. It shows progress of flexural deformation at one end of columns, and it may cause story collapse. The result is obtained from both loading tests.

ARTICLE INFO

Article history:
Received 6 January 2015
Accepted 10 March 2015

Keywords:
RC frame
Shear failure
Partial wall
Static loading test
Shaking table test

1. Introduction

Walls connected to the upper and the lower beams, however, apart from the both side columns, briefly called "partial walls" in this paper, are very popular as exterior walls in a large number of buildings, especially in apartment houses in Japan. In many cases, they had not been regarded as structural elements, because they did not satisfy the requirements for bearing walls, and their presence had been ignored in structural calculation until about decades ago for a long time. However, if slightly, they have a certain lateral stiffness and strength, therefore they have some influence on the structure, and it is necessary to grasp it adequately. In the previous paper, we reported the influence of the flexural yield type walls and concluded that elongation of the walls due to flexural yielding sometimes influenced much to the strength themselves and the behaviors of the beams connected to them. This paper deals with a case that the walls expected to fail due to shear prior to yield due to bending. In this case, it is considered that there is some fear that brittle failure of a wall at a certain story may cause the story collapse. The objective of this paper is to clarify influence of partial walls on reinforced concrete (RC) frames through a static loading test and a shaking table test.

2. Specimens

Two types of specimens, one of which is MW12 with 12 cm wide partial walls and the other is MW15 with 15 cm wide ones, were provided. The specimens for static loading test are named MW12-S and MW15-S by adding "S", and the specimens for shaking table test are named MW12-D and MW15-D by adding "D". The size and the reinforcement of the specimens for the both loading tests are the same as each other. A typical specimen (MW12-S) is shown in Fig. 1. The specimens are 1/8 scale models of one span and two story frames with a partial wall at mid-span at every story. The members have the dimensions as described in Table 1 and as detailed in Fig. 2. The walls are designed to fail due to shear before flexural yielding. By contrast, the beams and the columns are sufficiently strengthened against shear. Mechanical properties of the concrete and the reinforcement are indicated in Table 2.

3. Static Loading Test

The outline of the loading is illustrated in Fig. 1 above mentioned. In order to restrict the wall's axial elongation

* *Corresponding author*. Tel.: +81-3-5734-3108 ; E-mail address: hotta@arch.titech.ac.jp (H. Hotta)
ISSN: 2149-8024 / DOI: http://dx.doi.org/10.20528/cjsmec.2015.03.003

caused by their bending yield, a steel tube with sufficient stiffness is attached to the top of the specimens with pin support. Due to this treatment, the specimens show almost the same behavior as that on the lower part of middle-rise buildings. A constant axial force equivalent to 0.15 bDFc (25.1 kN) was loaded by vertically pulling PC bars running through the center of the columns. The both ends of the second story beam of the specimen was horizontally pulled and pushed with the same force.

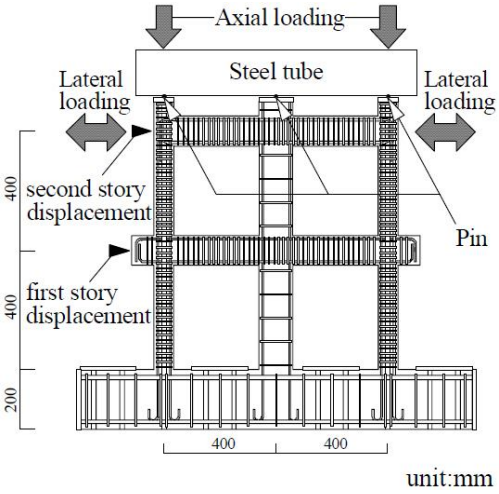

Fig. 1. Specimen (MW12-S) and outline of static loading.

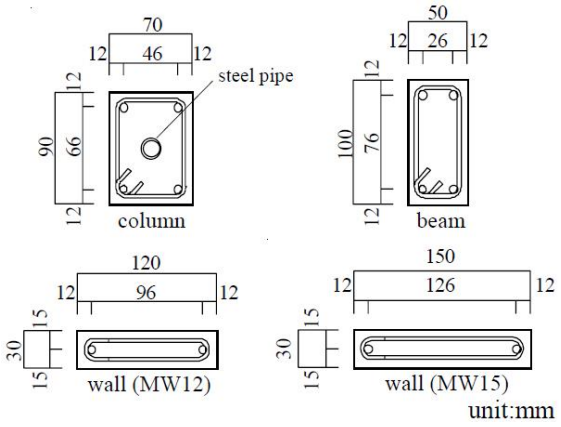

Fig. 2. Section of members.

Table 1. Section detail of members.

column	b D (mm)	90×70
	Main reinforcement	4-D6 pg=2.01%
	Hoop reinforcement	2-3φ @15 pw=1.05%
beam	b D (mm)	50×100
	Main reinforcement	4-D6 pg=2.53%
	Hoop reinforcement	2-3φ @18 pw=1.57%
wall (MW12)	b D (mm)	30×120
	Main reinforcement	2-D6 pg=1.76%
	Hoop reinforcement	2-3φ @79 pw=0.6%
wall (MW15)	b D (mm)	30×150
	Main reinforcement	2-D6 pg=1.41%
	Hoop reinforcement	2-3φ @79 pw=0.6%

Relationships between the lateral load and the displacement of the second story are indicated in Fig. 3. MW12-S recorded the maximum lateral load (27.2 kN) in the third loading loop, and the second story wall and the first story wall fell in shear failure in turn in the fourth loading loop. MW15-S recorded the maximum lateral load (32.0 kN) in the third loading loop, and soon, the wall of the second story fell in shear failure. And the wall of the first story fell in bond failure in the fourth loading loop.

Table 2. Mechanical properties of the materials.

For static loading test (MW12-S,MW15-S)			
Concrete			
Age	Compressive strength (MPa)	Tensile strength (MPa)	Young's modulus (MPa·10³)
28	26.6	3.05	27.0
35	28.4	3.26	25.9
Reinforcing bars			
Size	Compressive strength (MPa)	Tensile strength (MPa)	Young's modulus (MPa·10³)
D6	347	506	187
3φ	630	680	213
For shaking table test (MW12-D,MW15-D)			
Concrete			
Age	Compressive strength (MPa)	Tensile strength (MPa)	Young's modulus (MPa·10³)
29	30.0	2.96	27.2
Reinforcing bars			
Size	Compressive strength (MPa)	Tensile strength (MPa)	Young's modulus (MPa·10³)
D6	334	495	197
3φ	493	663	201

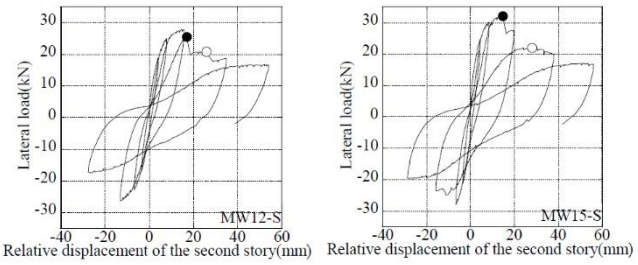

Fig. 3. The relationships between the lateral force and the displacement.

Relationships between the story drift angle of the first story and that of the second story are shown in Fig. 4. Dots ∘ and • indicate the point the first and the second story walls failed. It is recognized the story drift of the second story increased compared with that of the first story after the second story wall failed. It shows progress of flexural deformation at the second story column-base. This tendency is outstanding in MW15-S. That means, the walls of MW15-S are stiffer than those of MW12-S,

therefore the difference of story stiffness between the first story and the second story appears more clearly after one of the partial walls fails.

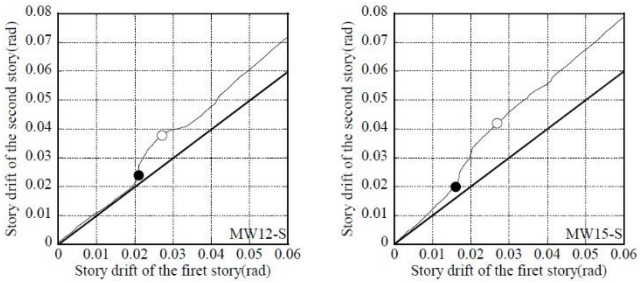

Fig. 4. Relationship between story drift of the second story and the first story.

4. Shaking Table Test

The outline of the setup is illustrated in Fig. 5. How the mass is connected to the specimen is detailed in Fig. 6. A H-shaped steel is connected at the top of the column of the specimen by pin connections. The total mass of the additional mass is 1.97 tons. Its center of gravity is almost coincident with the central point of the second story beam, therefore it can be said that the loading is similar to that of the static loading test. The H-shaped steel also plays the role of restricting the walls' axial elongation. As the axial force of the columns due to the mass is shorter than design axial compression of 0.15 bDFc (28.4 kN), the lack is filled up by pulling PC bars running through the columns. Input ground motion is NS component of JMA KOBE wave. As the size of the specimen is 1/8 times as large as a practical frame, amplitude of the wave is reduced to 1/8. The compression ratio of time axis is 3/10. The wave is named briefly "Kobe" in this paper. The natural period of the specimen including the additional mass is about 0.10 sec., therefore the specimen corresponds to a building with natural period of 0.33 sec., namely, a 5-6 story middle-rise building in actual size. A typical input ground motion is shown in Fig. 7. Run table is shown in Table 3.

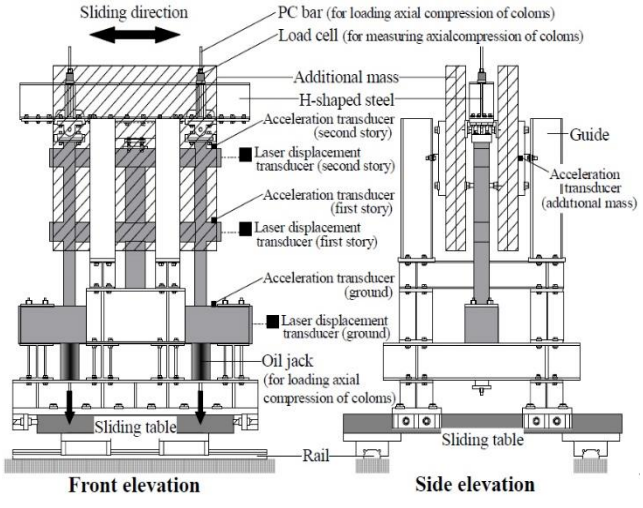

Fig. 5. Outline of loading setup and measuring.

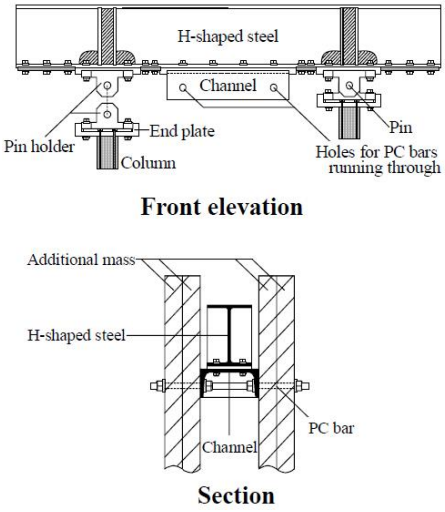

Fig. 6. Detailed drawing of connection to specimens of additional mass.

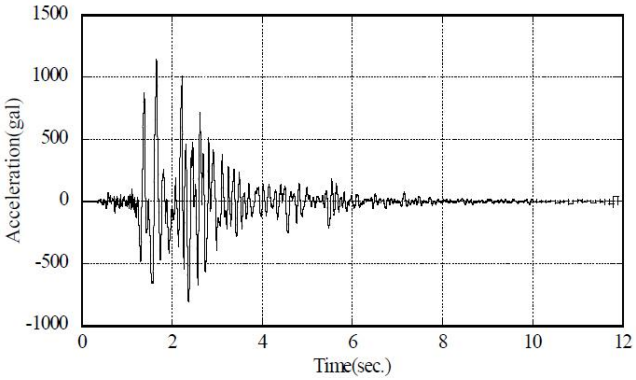

Fig. 7. Input ground motion (Kobe·1.0).

Table 3. Run table of shaking table test.

Run	MW12-D		MW15-D	
1	Kobe	0.1	Kobe	0.1
2	Kobe	0.3	Kobe	0.3
3	Kobe	0.5	Kobe	0.5
4	Kobe	0.7	Kobe	0.7
5	Kobe	1.0	Kobe	1.0
6	Kobe	1.2	Kobe	1.2
7	Kobe	0.5	Kobe	0.5
8	Kobe	0.7	Kobe	0.7
9	-	-	Kobe	1.0
10	-	-	Kobe	1.2

The relationships between the lateral force and the displacement are shown in Fig. 8 for several input level, Run-4, -5, -6 and -8. In the figure, the lateral force means the one obtained by multiplying the recorded absolute acceleration of the additional mass by the mass of 1.97 tons, which is equivalent to the sum of restoring force and damping force, and the displacement is the relative displacement between the stub and the second floor. Until Run-3, both specimens showed almost elastic behavior. During Run-4, the both specimens went into inelastic

region and hysteresis loop gradually shifted to slip type. As for Run-5, a number of shear cracks are observed in the walls after shaking for both the specimens, however, they had not yet experienced the strength degradation due to shear failure of the walls. During Run-6, the walls at both the stories were failed due to shear in both the specimens. As shown in Fig. 9, it can be recognized that the elongation of the walls rapidly decreased after the time indicated by dots ∘ and •, and it is considered that the walls were failed at the time indicated by the dots, respectively. According to the above consideration, as for the specimen MW12-D, the wall at the lower story failed at first (1.53 sec) and then the upper story wall failed (1.61 sec), and as for MW15-D, the upper wall failed at first (1.53 sec) and then the lower one (1.63 sec.) As for Run-8, both specimens exhibited considerable slip behavior, and the restoring force did not reach the residual lateral strength of the specimens.

Story drift angle of the first story is compared with that of the second story in Fig. 10. It is recognized that the story-drift at the story where the wall failed former rapidly increased compared with the other during two times of the shear failure of the walls. It is the same results as provided in the static loading test, though the wall failed earlier was different according to the specimens. In the specimens for the shaking table test, two failure occurred in a very short period of 0.1 sec and the columns were designed still little stronger than the beams, therefore, the influence of the brittle behavior of the wall is limited small. The reason they occurs in a short period can be considered that shear failing of one wall releases the restriction of the elongation for the other wall, and that weaken the shear strength of the wall, however, if less stronger columns are used, the attention should be continuously paid on this problem, because there is still some fears the brittle failure of the wall eventually cause story collapse.

Equivalent damping ratio evaluated each half loop as shown in Fig. 11 is plotted in Fig. 12 for both the specimens. This includes the ordinary viscous damping ratio because the lateral force is the sum of restoring force and damping force in the hysteresis previously described. The horizontal axis of Fig. 12, x_{max} corresponds to that in Fig. 11 and it is almost equivalent to the lateral displacement of the story when x_{max} is smaller than about 10mm, therefore the plots in Fig. 12 are the equivalent damping ratios before the wall fails. In spite that the walls do not fail, they exhibited 0.1 and more. The damping ratios for MW12-D are totally higher than those for MW15-D.

The relationships between the lateral load and the displacement under the static loading test (solid line) and the relationships between the lateral force and the displacement under the shaking table test (■ and □) are shown in Fig.13. Dot ■ means the time when the specimens recorded the maximum lateral load during each Run from -1 to -6, and dot □ means the time when the specimens recoded the maximum displacement of the second story during Run-6. Though the lateral force is the sum of restoring force and damping force, the velocity of deformation is almost 0 when the dots ■ and □ are recorded, therefore damping force included in the lateral force at the dots ■ and □ is almost 0.

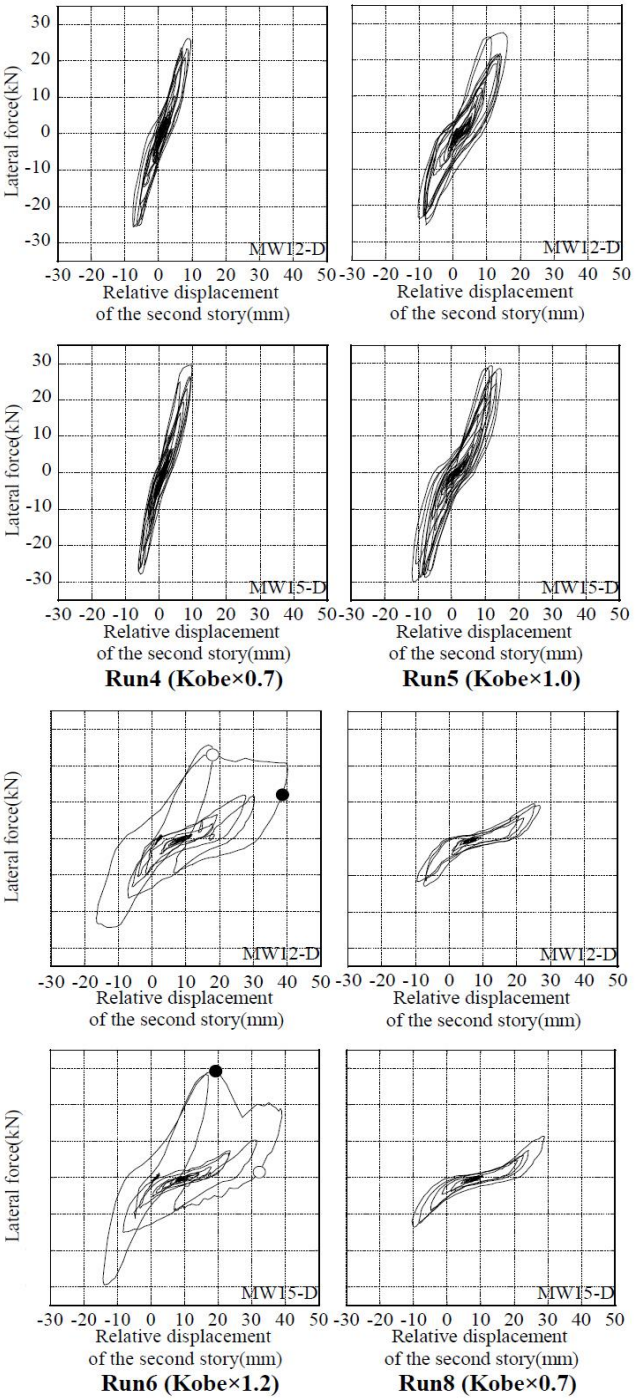

Fig. 8. The relationships between the lateral force and the displacement.

The specimens' mechanical properties for the both loading tests are similar. By the above consideration, the lateral force recorded through the shaking table test can be simply compared with the lateral load recorded through the static loading test. Generally the results under the both loading tests are coincident with each other in MW12 and MW15. The displacement when the specimens show the peak restoring force in the both loading tests are also coincident with each other. In other words, the deformation limit of the walls does not depend on a method of the loading. Under the shaking table test the displacement increases rapidly after the walls failed than under static loading test.

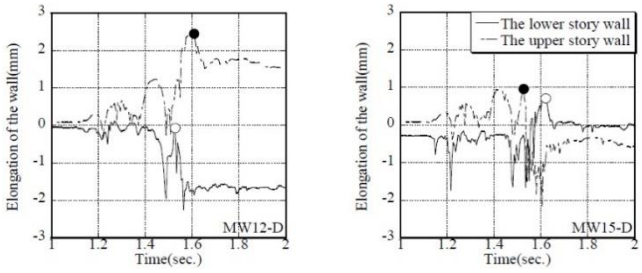

Fig. 9. Time history of the elongation of the walls (Run-6).

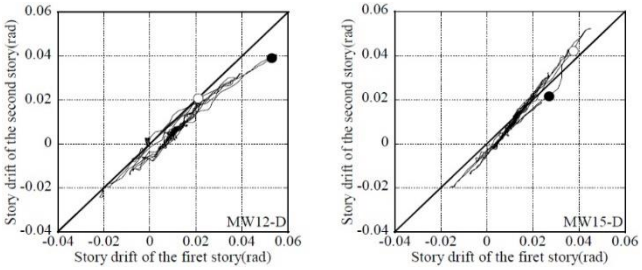

Fig. 10. Relationship between story drift of the second story and the first story (Run-6).

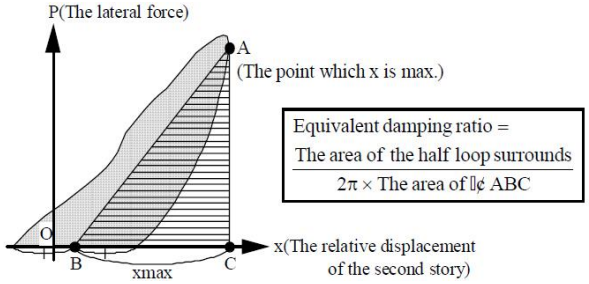

Fig. 11. Evaluation of equivalent damping.

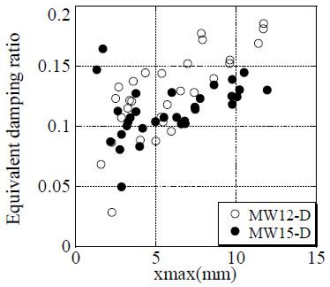

Fig. 12. Relationship between equivalent damping ratio and x_{max} (Run-3, -4, -5).

5. Conclusions

- Shear failure of a wall makes the story drift at the story where the failed wall exists progress more than other story. However whether that cause the story collapse has not clarified yet. It is necessary to do continuous investigation on this issue.
- Equivalent damping ratio more than 0.1 is expected for RC frames with the partial walls before exhibiting the ultimate lateral strength.
- The relationships between the force and the displacement under the static loading test and the shaking table test are coincident with each other. And the deformation limits of the walls under the two loading test are coincident, too.

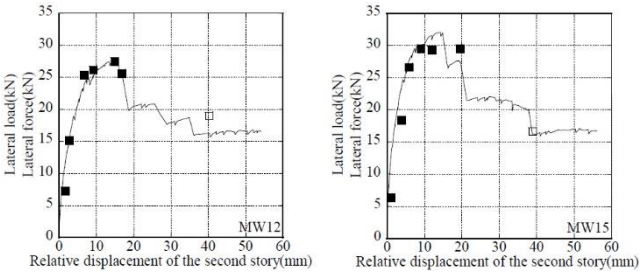

Fig. 13. Outline of loading setup and measuring.

References

Hotta H, Tsunoda T (2004a). An experimental study on influence of mullion-type wall of predominant bending failure in reinforced concrete frame. *Proceedings of the 1st International Conference on Urban Earthquake Engineering*, Yokohama, Japan, 105-111.

Hotta H, Tsunoda T (2004b). An experimental study on influence of mullion-type wall of predominant bending failure in load-carrying capacity and deformation efficiency of reinforced concrete frame. *Journal of Structural and Construction Engineering (Transaction of Architectural Institute of Japan)*, 582, 131-136 (in Japanese).

Hotta H, Kimura T (2005). An Analytical study on influence of multi-story mullion-type walls of predominant bending failure in reinforced concrete structure. *Journal of Structural and Construction Engineering (Transaction of Architectural Institute of Japan)*, 591, 123-128 (in Japanese).

Challenge Journal of Structural Mechanics

A modified member stiffness procedure for dynamic progressive collapse analysis of planar frames

Griengsak Kaewkulchai *, Sdhabhon Bhokha

Department of Civil Engineering, Ubon Ratchathani University, Warin Chamrap, 34190 Ubon Ratchathani, Thailand

ABSTRACT

A computer program for progressive collapse analysis of planar frames is under development. The software has a capability to analyze structures after failures of members in which failure can occur at one or both ends of a member. When an end of a member fails, the failed end separates from the main structure and becomes discontinuous. In this paper, a modified member stiffness procedure with releases of end forces to track the response of a failed end is discussed. The procedure utilizes a condensation process of the element stiffness matrix of the failed member. An example in applying the modified member stiffness procedure is given to show that the assembly process for the stiffness matrix and the applied force vector of the main structure does not change. In addition, the Equation solver still determines the same number of unknown degrees of freedom. Accordingly, this approach provides a convenient, simple, yet efficient means of keeping track of all failed members for progressive collapse analysis of frame structures.

ARTICLE INFO

Article history:
Received 5 January 2015
Accepted 13 March 2015

Keywords:
Progressive collapse
Building collapse
Dynamic analysis
Condensation
Frames

1. Introduction

Progressive collapse is a type of collapse that can be defined as a chain reaction of failures initiated by a loss of one or more supporting elements. Thus far, an analysis technique known as the "Alternate Load Path" method has been employed for investigating the potential of progressive collapse in buildings. The method has been adopted by many current design codes and standards in USA (GSA 2000; IBC 2000; DOD 2001). Although the importance of considering dynamic effects has been shown (Pretlove et al., 1991; Kaewkulchai and Williamson, 2002) and some design provisions have suggested the use of dynamic analysis in conjunction with the alternate load path method (GSA 2000; DOD 2001), how to perform such analysis still at large relies on engineering judgment.

For the current research study being conducted, a computer program for dynamic progressive collapse analysis of planar frames is under development. The software has a capability to analyze structures after failures of members in which failure can occur at one or both ends of a member. When an end of a member fails, the failed end separates from the main structure and becomes discontinuous. In this paper, a modified member stiffness procedure with releases of end forces to track the response of a failed end is discussed. The procedure utilizes a condensation process of the element stiffness matrix of the failed member. An example in applying the modified member stiffness procedure is given to show that using the modified member stiffness approach can result in a simple, yet efficient analysis routine for analyses of frame structures after member failure.

2. A Computer Program

Two General description of the developed software is given in this section. A more detailed explanation of these subjects has been given elsewhere (Kaewkulchai and Williamson, 2004). The software utilizes the conventional direct stiffness method for the main analysis routine. An implicit direct integration scheme, the Newmark-beta method is employed to solve the governing

* *Corresponding author*. E-mail address: griengsak.k@oup.ubu.ac.th (G. Kaewkulchai)
ISSN: 2149-8024 / DOI: http://dx.doi.org/10.20528/cjsmec.2015.03.004

equations of dynamic equilibrium coupled with Newton-Raphson iterations for carrying out the nonlinear analyses. The program assumes the use of a classical or proportional (Rayleigh) damping matrix along with the use of a lumped mass matrix. Geometric nonlinearity (P-Δ effect) is taken into account by using a simplified geometric stiffness matrix. For material nonlinearity, a lumped plasticity model for beam-column elements is applied in which inelasticity is assumed to occur only at element ends or hinges (Fig. 1). Effects of strength and stiffness degradation of members are modeled by means of a damage model. The damage model utilizing a damage index at each member end is used to determine the onset of member end failure.

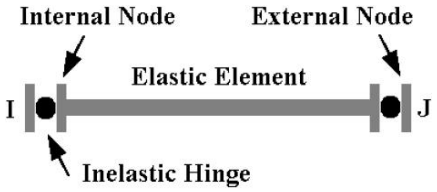

Fig. 1. Inelastic beam-column element.

The software has a capability to analyze frame structures after failures of members. When an end of a member fails, the failed end separates from the main structure and becomes discontinuous. To continue the analysis, an additional node at the failed end may be introduced. Because three new degrees of freedom associated with the new node are added to the structure, the system of equations becomes larger. Hence, the analysis requires more computational effort, particularly when there are many failed ends. In addition, changing the dimensions of all system matrices during the course of analysis is required, resulting in expensive computer time for transferring data between matrices. Also, new definitions for element connectivity must be established. As a result of the drawbacks associated with adding a new node to the definition of the structural model, in the current computer program the analysis continues in an efficient manner through the use of a modified member stiffness procedure with releases of end forces. Systematically, this approach provides a convenient means of keeping track of all failed members, and the main analysis routine is not greatly altered. The modified member stiffness procedure is described in the following section.

3. A Modified Member Stiffness Procedure

As mentioned in the previous section, the modified member stiffness procedure is employed to track the response of a failed end. The modified member stiffness approach utilizes a condensation process of the element stiffness matrix. Static condensation for a beam element is well established in the literature (e.g, Felton and Nelson, 1997). For the 2-D beam-column element under consideration (Fig. 2), all three degrees of freedom at one end of an element are released (u_1-u_3 or u_4-u_6) because of the failure of an end. When releasing one end, the element forces at that location become zero. Because these force values are known, the corresponding displacement quantities can be expressed in terms of the displacements at the other end of the element using matrix condensation.

Fig. 2. Element end displacements and forces.

Considering the response of a beam-column element in which one of the ends has failed, the incremental equilibrium equations of the failed element can be written as follows:

$$\Delta R = K\Delta_u + \Delta R_F \,. \tag{1}$$

For expressive reason, assume that failure takes place at the right end of the beam-column element in Fig. 2. Thus, two sets of matrix equations result and Eq. (1) can be rewritten as

$$\begin{Bmatrix} \Delta R_c \\ \Delta R_r \end{Bmatrix} = \begin{bmatrix} K_{cc} \,|\, K_{cr} \\ K_{rc} | K_{rr} \end{bmatrix} \begin{Bmatrix} \Delta u_c \\ \Delta u_r \end{Bmatrix} + \begin{Bmatrix} \Delta R_{Fc} \\ \Delta R_{Fr} \end{Bmatrix}, \tag{2}$$

where subscripts c and r refer to 'contracted' and 'released', respectively.

From Eq. (2), the contracted set consists of incremental force and displacement vectors corresponding to the element degrees of freedom 1 through 3 at the intact end. Similarly, the released set contains those for the element degrees of freedom 4 through 6 at the released end. Because the released element force vector ΔR_r is zero, the released displacement vector Δu_r can be written in terms of Δu_c as

$$\Delta u_r = -[K_{rr}]^{-1} \left[K_{rc}\Delta u_c + \Delta R_{Fr}\right], \tag{3}$$

Accordingly, the incremental equilibrium equations for the contracted set can be expressed by

$$\Delta R_c = \bar{K}_{cc}\Delta u_c + \Delta \bar{R}_{Fc} \,, \tag{4}$$

where $\bar{K}_{cc} = [K_{cc} - K_{cr}\, K_{rr}^{-1}\, K_{rc}]$ is the modified member stiffness matrix and $\Delta\bar{R}_{Fc} = [\Delta R_{Fc} - K_{cr}\, K_{rr}^{-1}\, \Delta R_{Fr}]$ is the incremental modified fixed-end force vector.

It can be seen from Eq. (4) that the use of $\bar{K}_{cc}$ and $\Delta\bar{R}_{Fc}$ requires no special process in accounting for the new degrees of freedom associated with the failed end during the assembly process for the stiffness matrix and the applied force vector of the main structure in which the degrees of freedom associated with the failed end can be calculated using Eq. (3).

The relationships derived in Eqs. (3) and (4), however, are based on an assumption of static equilibrium of the element, and therefore cannot apply for dynamic analyses of frame structures. Nonetheless, because the

Newmark-beta method for solving the governing equations of dynamic equilibrium is employed, similar equations, which are valid for dynamic analyses, can be developed. In the Newmark-beta method, the governing equations of dynamic equilibrium can be cast in terms of unknown displacements. Accordingly, dynamic effects in the response are accounted for, and the procedure outlined previously can be used with only slight modification.

Let us consider the governing equations of motion for a dynamic system which can be described by

$$M_s U'' + C_s U' + K_s U = P \,, \tag{5}$$

where U, U' and U'' are the displacement, velocity and acceleration vectors; M_s, C_s and K_s are the system mass, damping and stiffness matrices; P is the external applied force vector.

Then, the incremental equations of motion combined with the Newmark-beta method can be written as

$$\Delta P_{eff} = K_{s\,eff}\,\Delta U \,, \tag{6}$$

$$K_{s\,eff} = A_1 M_s + A_4 C_s + K_s \,, \tag{7}$$

$$\Delta P_{eff} = \Delta P + M_s\{A_2 U' + A_3 U''\} + C_s\{A_5 U' + A_6 U''\}, \tag{8}$$

where A_1 through A_6 are the Newmark constants.

Because the effective system stiffness matrix, $K_{s\,eff}$ and the effective incremental applied force vector, ΔP_{eff} is a result from the assembly process of each beam-column element, one can express the incremental equilibrium equations of an element, similar to Eq. (1) as follows:

$$\Delta R_{eff} = K_{eff}\Delta u + \Delta R_{eff\,F} \,, \tag{9}$$

$$K_{eff} = A_1 M + A_4 C + K \,. \tag{10}$$

Because the fixed-end forces are the negative values of the applied forces, the effective incremental fixed-end force vector, $\Delta R_{eff\,F}$, similarly to ΔP_{eff} (see Eq. (8)), is given as

$$\Delta R_{eff\,F} = \Delta R_F - M[A_2 v + A_3 a] - C[A_5 v + A_6 a] \,, \tag{11}$$

where v and a are the velocity and acceleration vectors of the element, while M and C are the element mass and element damping matrices.

By assuming the right end of the element failed, two sets of matrix equations result in Eq. (9) and the released displacement vector Δu_r from Eq. (3) can be rewritten as

$$\Delta u_r = -\left[K_{eff\,rr}\right]^{-1}\left[K_{eff\,rc}\,\Delta u_c + \Delta R_{eff\,Fr}\right]. \tag{12}$$

The derived equation for Δu_r is now based on dynamic equilibrium, and therefore, inertial effects are accounted for by using K_{eff} and $\Delta R_{eff\,F}$. Furthermore, similar to Eq. (4), the incremental equilibrium equations for the contracted set can be given by

$$\Delta R_{eff\,c} = \bar{K}_{eff\,cc}\,\Delta u_c + \Delta \bar{R}_{eff\,Fc} \,, \tag{13}$$

where $\bar{K}_{eff\,cc}$ is the modified member stiffness matrix and $\Delta \bar{R}_{eff\,Fc}$ is the incremental modified fixed-end force vector for dynamic equilibrium.

$$\bar{K}_{eff\,cc} = [K_{eff\,cc} - K_{eff\,cr}\,K_{eff\,rr}^{-1}\,K_{eff\,rc}] \,, \tag{14}$$

$$\Delta \bar{R}_{eff\,Fc} = [\Delta R_{eff\,Fc} - K_{eff\,cr}\,K_{eff\,rr}^{-1}\,\Delta R_{eff\,Fr}] \,. \tag{15}$$

Based on the discussion above, together with Eqs. (10) to (15), the procedure for dynamic progressive collapse analysis with the modified member stiffness approach only involves modification of the stiffness matrix and fixed-end forces of a failed member. Thus, Eq. (13) can be employed with the modified member stiffness matrix, $\bar{K}_{eff\,cc}$ and the modified fixed-end force vector, $\Delta \bar{R}_{eff\,Fc}$. These matrices correspond to the contracted degrees of freedom at the intact end.

With $\bar{K}_{eff\,cc}$ and $\Delta \bar{R}_{eff\,Fc}$, analysis after member failure can continue with little modification to the main analysis routine because no new degrees of freedom are added to the system. At the end of a converged time step, the released displacement vector Δu_r at the failed end of the member can be obtained from the contracted displacement vector Δu_c using Eq. (12). Thus, using the approach just outlined, the assembly process for the stiffness matrix and the applied force vector of the main structure does not change. In addition, the equation solver still determines the same number of unknown degrees of freedom. Accordingly, applying the modified member stiffness approach results in a simple, yet efficient analysis routine for analyses of frame structures after member failure.

4. Analysis Example

An example in applying the modified member stiffness procedure is given in this section. Results obtained from a dynamic analysis using this approach are compared with those obtained from a conventional dynamic analysis. For illustrative purpose, a fixed-fixed beam shown in Fig. 3 is used. Note that the beam is assumed to have elastic-perfectly plastic behavior.

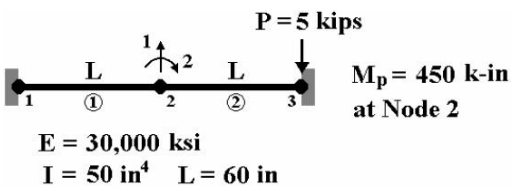

Fig. 3. A fixed-fixed beam modeled using two elements.

The fixed-fixed beam consists of two elements and two degrees of freedom as shown in Fig. 3. A point load, P of 5 kips acts at Node 3. Apparently, the system will not react because the point load is acting at a support. To illustrate the modified member stiffness method, the right end of member 2 is assumed to abruptly fail so that the

support is no longer available to resist loads. For a conventional dynamic analysis, a new node (Node 3) would need to be introduced; therefore two new degrees of freedom are introduced into the system. Hence, after failure at Node 3, the system can be analyzed by using an equivalent system having four degrees of freedom with a suddenly applied force, *P* at Node 3 as shown in Fig. 4.

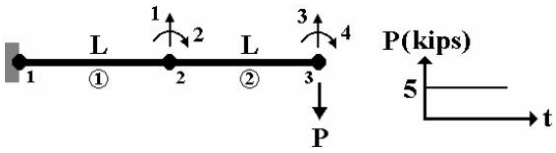

Fig. 4. An equivalent system with a suddenly applied force.

For a dynamic analysis using the modified member stiffness approach, however, only two degrees of freedom are required so that no new degrees of freedom are introduced to the system. The response, however, at the failed end can be obtained through Eq. (12). For the dynamic analyses performed, Δt = 0.01 sec and mass = 0.05 kips-s^2/in at each member end are used. In addition, rotational mass and damping are ignored. The results, obtained from a conventional dynamic analysis and a dynamic analysis using the modified member stiffness approach, are compared in Fig. 5.

Figs. 5(a-b) show the response of four degrees of freedom, 1 to 4. As seen in the graphs, the difference between the results obtained from the conventional dynamic analysis and the modified member stiffness approach is negligible. Similarly, bending moments and shear forces of members 1 and 2 obtained from the two approaches are nearly identical. Hence, applying the modified member stiffness approach results in a simple, yet efficient analysis routine for dynamic analyses of frame structures after member failure.

5. Conclusions

In recent years, progressive collapse has gained much interest due to severe building collapse. An analysis technique known as the "Alternate Load Path" method generally based on a static approach, has been employed for investigating the potential of progressive collapse in buildings by many current design standards. Although considering dynamic effects has been shown to be significant for the analysis of progressive collapse, how to perform such analysis is simply based on engineering judgment. For the current study, a computer program for dynamic progressive collapse analysis of planar frames is under development. The software has a capability to analyze structures after failures of members.

In this paper, a modified member stiffness procedure with releases of end forces to track the response of a failed end of members was discussed. An example in applying the modified member stiffness procedure was also given. The described approach to track the response of failed ends was simple, yet efficient to employ for dynamic collapse analyses of planar frame structures.

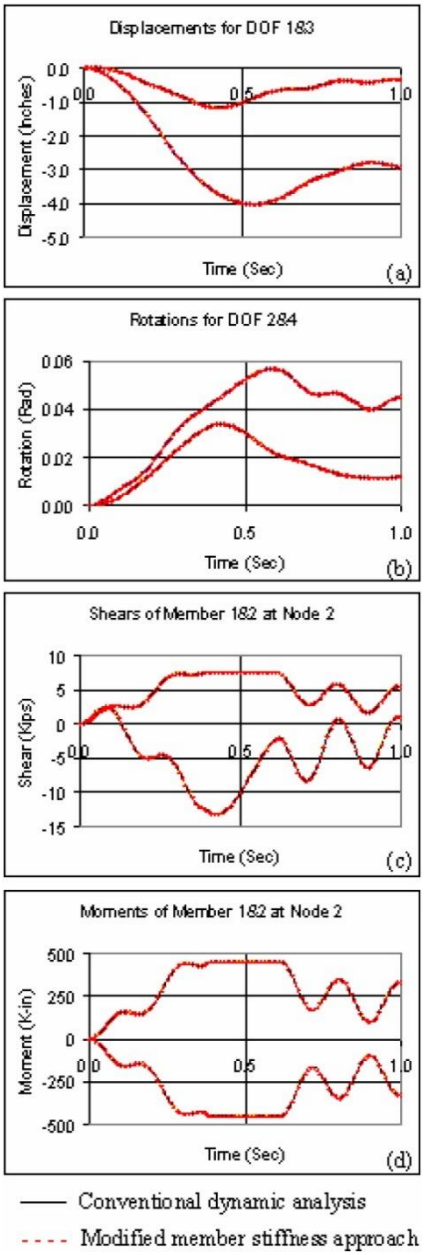

Fig. 5. Comparisons of the obtained results.

References

DoD (2001). DoD Interim Antiterrorism/Force Protection Construction Standards – Progressive Collapse Design Guidance. Department of Defense, Washington, DC.

Felton LP, Nelson RB (1997). Matrix Structural Analysis. Wiley & Sons, Inc., New York.

GSA (2000). Progressive Collapse Analysis and Design Guidelines for New Federal Office Buildings and Major Modernization Projects. General Services Administration, Washington, DC.

IBC (2000). International Building Code. International Code Council, USA.

Kaewkulchai G, Williamson EB (2002). Dynamic progressive collapse of frame structures. *The 15th Engineering Mechanics Division Conference*, ASCE, New York.

Kaewkulchai G, Williamson EB (2004). Beam element formulation and solution procedure for dynamic progressive collapse analysis. *Computers and Structures*, 82(7-8), 639-651.

Pretlove AJ, Ramsden M, Atkins AG (1991). Dynamic effects in progressive failure of structures. *International Journal of Impact Engineering*, 11(4), 539-546.

Challenge Journal of Structural Mechanics

Seismic analysis of interlocking mortarless hollow block

Farzad Hejazi *, Jamalodin Noorzaei, Abang Abdullah Abang Ali, Mohd Saleh Jaafar

Department of Civil Engineering, University Putra Malaysia, 43300 Serdang, Malaysia

ABSTRACT

Various types of interlocking mortarless (dry-stacked) block masonry systems have been developed worldwide. However, the characteristics of dry joints under compressive load, and their effect on the overall behavior of the interlocking mortarless system, are still not well understood. This paper presents an investigation into the dry-joint contact behavior of masonry and the behavior of interlocking mortarless hollow blocks wall construction subjected to seismic excitation. In the system developed, the blocks are stacked on one another and three-dimensional interlocking protrusions are provided in the blocks to integrate the blocks into walls. The response of the mortarless hollow block wall with respect to acceleration displacement and stress have been discussed.

ARTICLE INFO

Article history:
Received 6 January 2015
Accepted 16 March 2015

Keywords:
Masonry systems
Seismic analysis
Mortarless block
Interlocking block
Finite element method

1. Introduction

Interlocking mortarless load bearing hollow block system is different from conventional mortared masonry systems in which the mortar layers are eliminated and instead the block units are interconnected through interlocking protrusions and grooves. Numerous analytical models have been developed to simulate the behavior of different types of structural masonry systems using Finite element method. Two main approaches have been employed in the masonry modeling depending on the type of the problem and the level of accuracy. The macro-modelling approach intentionally makes no distinction between units and joints but smears the effect of joints presence through the formulation of a fictitious homogeneous and continuous material equivalent to the actual one which is discrete and composite (Lotfi and Shing, 1991; Cerioni and Doinda, 1994; Zhuge et al., 1998). The alternative micro-modelling approach analyzes the masonry material as a discontinuous assembly of blocks, connected to each other by joints at their actual position, the latter being simulated by appropriate constitutive models of interface (Suwalski and Drysdale, 1986; Ali and Page, 1988; Riddington and Noam, 1994). An extensive critical review for the analytical models of different masonry systems can be found in the performed study done by Alwathaf et al. (2003).

The complex interaction between block units, dry joint and grouting material has to be well understood under different stages of loading; i.e. elastic, inelastic and failure. For interlocking mortarless masonry systems, very limited FE analyses have been reported in the literature (e.g., Oh, 1994; Alpa et al., 1998).

The existing FE analyses are simplified and hence show inaccurate prediction for the structural response of the masonry systems compared to actual behavior of the systems found experimentally. Furthermore, the existing models ignore the interaction between masonry block units, mortarless joint and grout as well as are incapable of simulating the failure mechanism of the masonry system.

In this study, a finite element model is proposed and a program code is developed to predict the behavior of the system under compression load. The developed contact relations for dry joint within specified bounds can be used for any mortarless masonry system efficiently with less computational effort. The bond between block and grout is considered to simulate the deboning and slipping of the block–grout interface. Furthermore, the stress–strain behavior of masonry blocks and grout materials under compression for uniaxial and biaxial stress state was modelled.

* *Corresponding author*. E-mail address: farzad@fhejazi.com (F. Hejazi)
ISSN: 2149-8024 / DOI: http://dx.doi.org/10.20528/cjsmec.2015.03.005

2. Modelling of Mortarless Joint

In present study, the hollow prisms modelled using eight-noded isoparametric elements to simulate the masonry constituents, are shown in Fig. 1(a). Six-noded isoparametric interface element of zero thickness located between material elements to model the interface characteristics of the dry joint and bond between blocks are represented in Figs. 1(b-c), respectively. Fig. 2 shows the finite element geometric model of considered wall that was constructed by hollow blocks. Dimension of this model are 3 m width and 3 m height assumed. Therefore by considering the dimensions of each prism (30 cm with and 20 cm height), there are 10 prisms in horizontal and 15 prisms of hollow block in vertical direction.

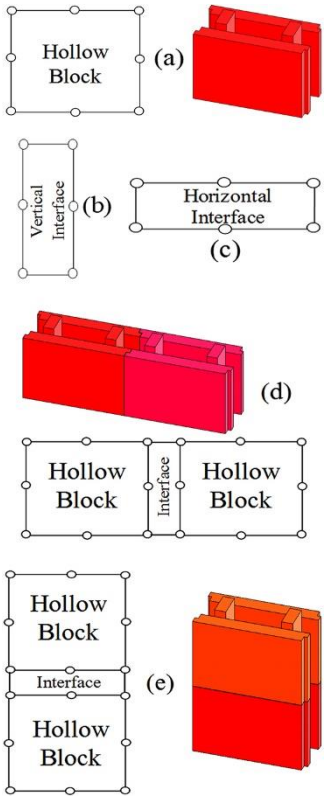

Fig. 1. (a) 8 node elements that was used for modeling of hollow block prism. (b) 6 node elements that was used for modeling of zero thickness vertical interface. (c) 6 node elements that was used for modeling of zero thickness horizontal interface. (d) Connection of two horizontal hollow block elements with vertical interface. (e) Connection of two vertical hollow block elements with horizontal interface.

In this finite element mesh as shown in Fig. 1(d) vertical dry joint between 2 horizontal block has been modelled by 6 node zero thickness vertical interface element and horizontal dry joint between 2 vertical block has been modelled by 6 node zero thickness horizontal interface element (Fig. 1(e)).

The considered wall is assembled by 150 blocks elements and 140 interface elements and model prepared by 865 elements and 2400 nodes. Therefore the final finite element mesh of wall is shown in Fig. 3.

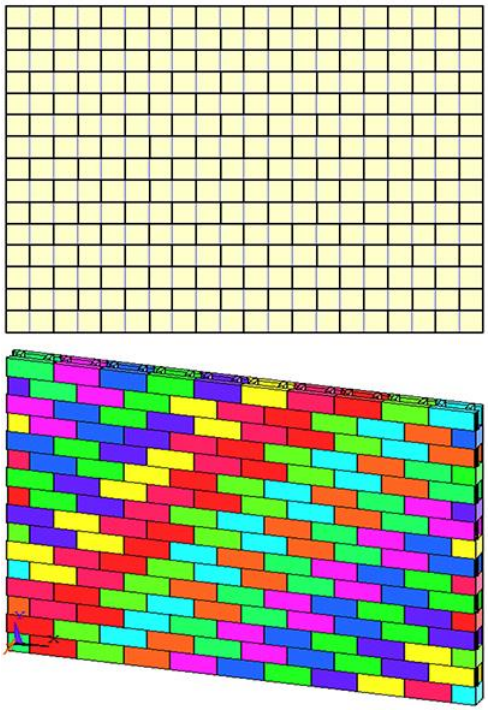

Fig. 2. Geometry of considered wall with 3 m width and 3 m height.

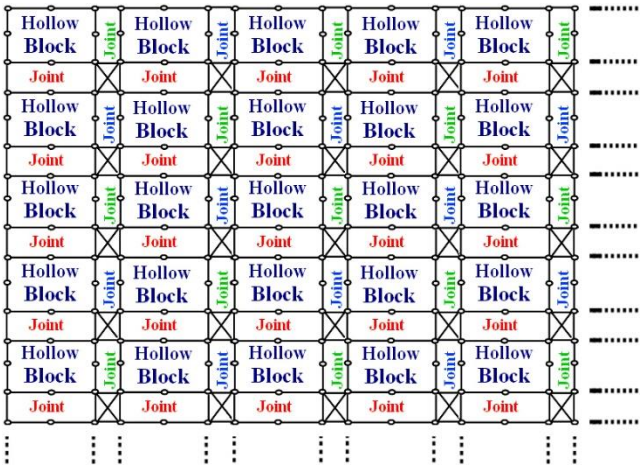

Fig. 3. Finite element model of hollow block wall.

3. Finite Element Analyses

A finite element program code has been developed to implement the proposed mortarless masonry model under seismic loading. Time history dynamic analysis of wall by imposing of suitable earthquake record for Malaysia and Indonesia are performed and shown in Fig. 4.

The time step of Malaysia earthquake record is 0.02 sec and duration of that is 20 sec and time step and duration of Indonesia record is 0.01 sec and 10 sec, respectively. Deformation of wall in imposing Malaysia and Indonesia earthquake excitation is shown in Fig. 5.

As seen in Fig. 5, top nodes of wall have high displacement in comparison with bottom nodes of wall and maximum displacement of wall occurs in the last top row of wall.

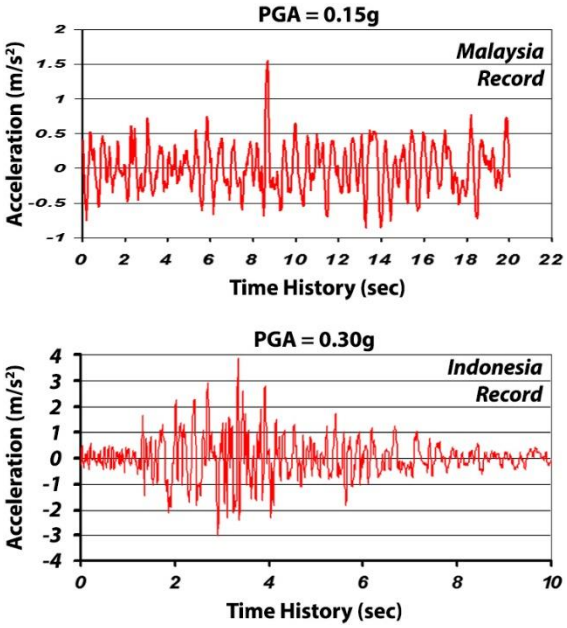

Fig. 4. Earthquake acceleration record for Malaysia and Indonesia.

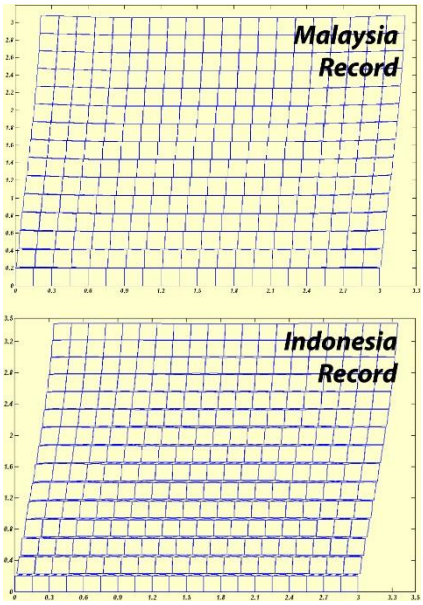

Fig. 5. Deformation of hollow block wall in Malaysia and Indonesia earthquake excitation (10 times exaggeration in *x* and *y* directions).

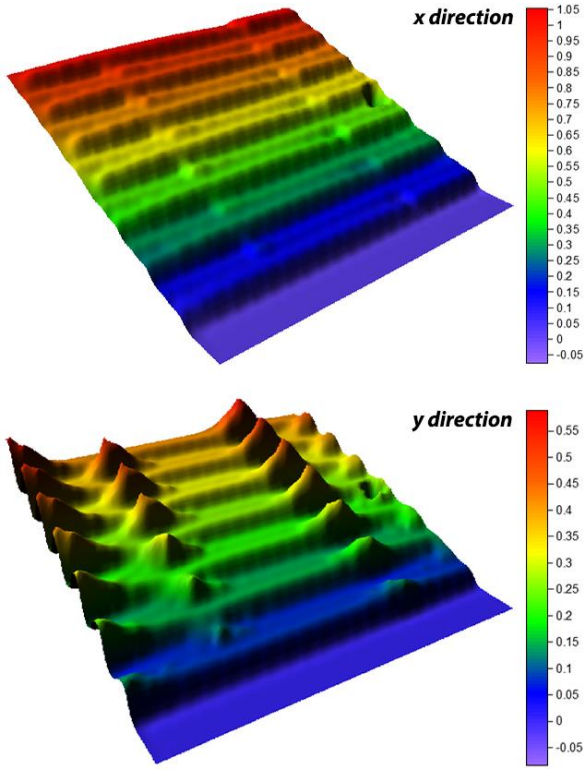

Fig. 6. Malaysia peak displacements in *x* and *y* directions (cm).

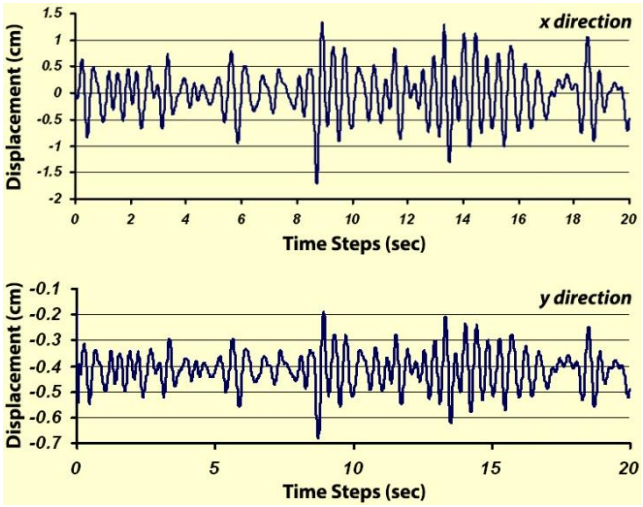

Fig. 7. Time-displacement history of top node of wall in *x* and *y* directions (cm).

4. Results and Discussion

4.1. Malaysia record excitation

Peak value of nodes' displacement in *x* and *y* directions during the earthquake excitation is determined by dynamic analyzes and values of that are plotted in Fig. 6.

The maximum displacement in *x* direction is 1.73 cm and in *y* direction is 0.71 cm. These values were less than allowable displacement for a masonry wall which were acceptable. The time history response and movement of wall during Malaysia earthquake load excitation, at top node of wall in *x* and *y* directions are shown in Fig. 7.

Peak value of each element stress *x* and *y* directions during the time steps of earthquake excitation are shown in Fig. 8. The maximum principle stress in *x* and *y* directions at bottom of wall is equal to 0.05222 and 0.1701 MPa.

Stress at bottom of wall is shown in Fig. 9. The stress values are very small because just single story building with very lightweight roof has been considered. Also just horizontal component of earthquake load imposed to wall and vertical component is neglected. So, maximum stresses in wall members are very smaller than the strength of blocks. Therefore the hollow block can be resist Malaysia earthquake excitation with allowable deformation and stress.

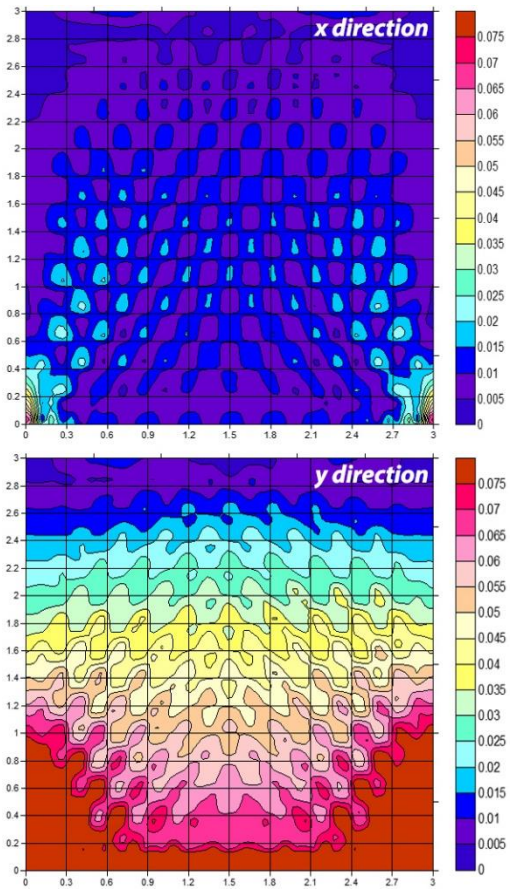

Fig. 8. Peak stresses in *x* and *y* directions (MPa).

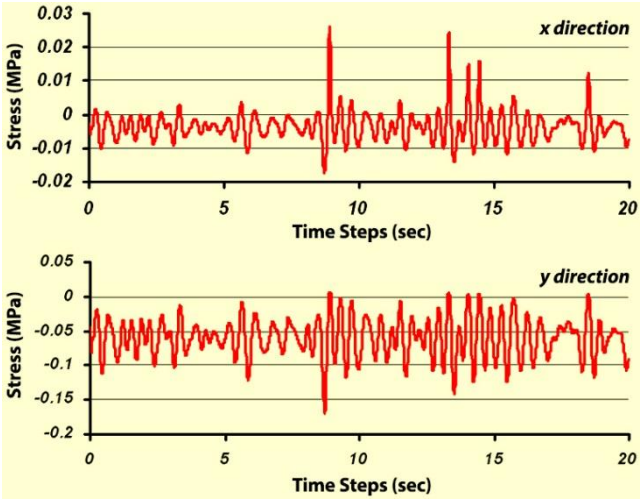

Fig. 9. Time-stress history of corner element in bottom of wall (MPa).

4.2. Indonesia record excitation

Peak value of nodes' displacement in *x* and *y* directions during the earthquake excitation is determined by dynamic analyzes and values of that are plotted in Fig. 10.

The maximum displacement in *x* direction is 2.13 cm and in *y* direction is 0.831 cm. The time history response and movement of wall during Indonesia earthquake load excitation, at top node of wall in *x* and *y* directions is shown in Fig. 11.

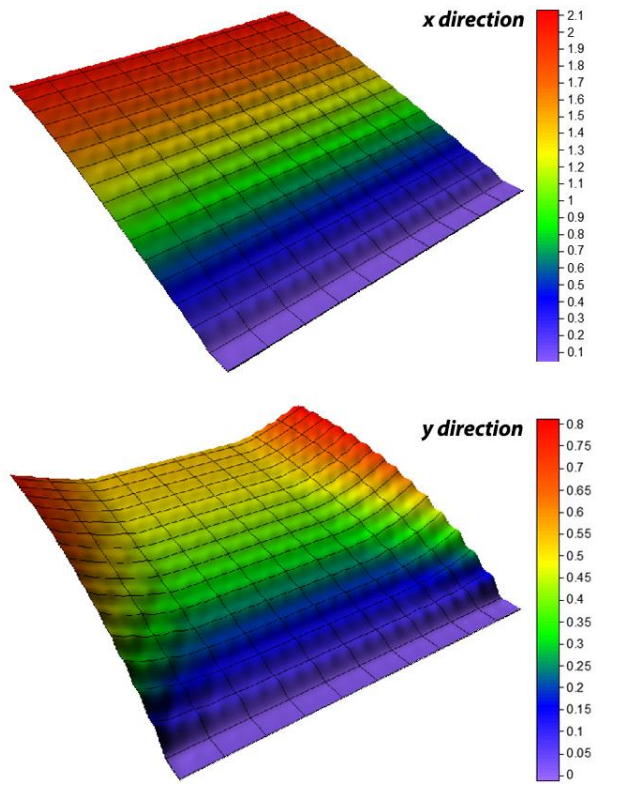

Fig. 10. Indonesia peak displacements in *x* and *y* directions (cm).

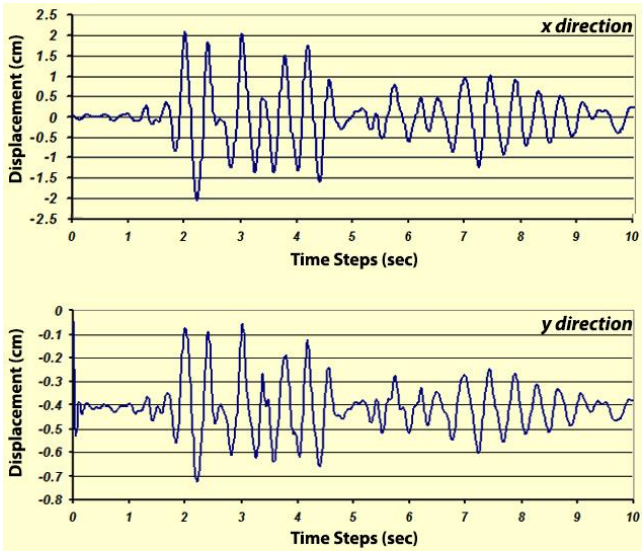

Fig. 11. Time-displacement history of top node of wall in *x* and *y* directions (cm).

The values of maximum displacements of wall are exceeded from allowable displacement for masonry wall, and then it is not acceptable.

Fig. 12 shows stress distribution in the wall subjected to Indonesia earthquake record. The maximum principle stress in *x* and *y* directions at bottom of wall is equal to 0.072 and 0.19 MPa.

Variation of stress at bottom of wall in duration of subjected earthquake has been shown in Fig. 13. Apparently the value of stress is small value and less than strength of hollow blocks.

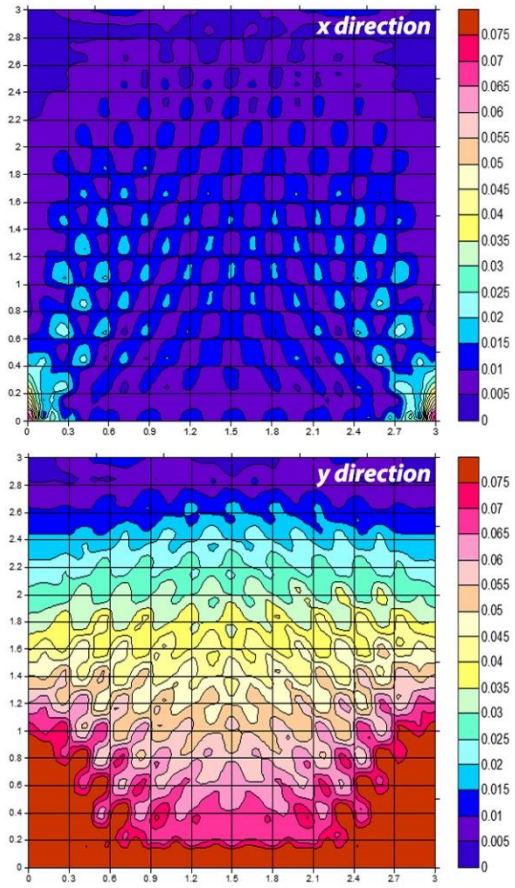

Fig. 12. Peak stresses in *x* and *y* directions (MPa).

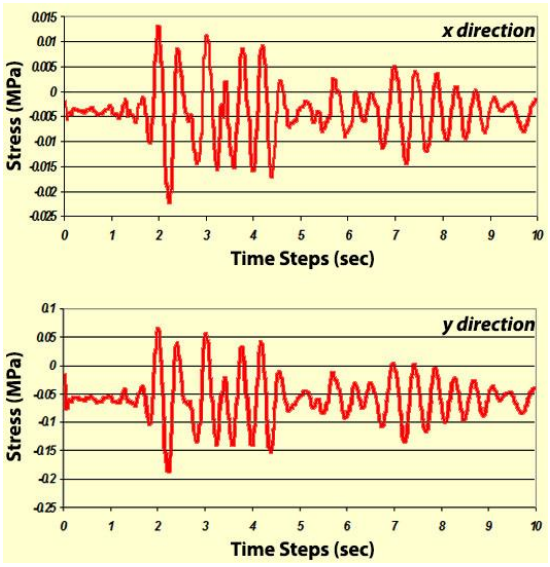

Fig. 13. Time-stress history of corner element in bottom of wall (MPa).

Therefore the wall can resist the stress but displacements of wall exceed the allowable values and it cannot satisfy the deformation limit.

5. Conclusions

Based on the foregoing analysis and discussion of the test results from this investigation, several conclusions can be drawn as follows.

- Finite element model of mortarless block masonry system has been developed. The model is at micro-level which includes the modeling of masonry materials, mortarless dry joint and block-grout interface behavior.
- The interlocking keys provided for this system were able to integrate the blocks into a sturdy wall and can replace the mortar layers that are used for conventional masonry construction in low seismic area.
- Considered wall system can be resist in Malaysia earthquake record excitation (PGA=0.15g, low seismic hazard level) but in Indonesia earthquake record excitation (PGA=0.39g, high seismic hazard level), displacement of wall is exceed allowable values. Therefore this type of wall that constructed by explained hollow blocks just resist low seismic excitation.

References

Ali SS, Page AW (1988). Finite element model for masonry subjected to concentrated loads. *ASCE's Journal of Structural Engineering*, 114(8), 1761-1784.

Alpa G, Gambarotta L, Monetto I (1998). Dry block assembly continuum modelling for the in-plane analysis of shear walls. *Proceeding of the 4th International Symposium on Computer Methods in Structural Masonry,* E & FN, Spon, 111-118.

Alwathaf AH, Thanoon WAM, Noorzaei J, Jaafar MS, Abdulkadir MR (2003). Analytical models for different masonry systems. *Critical Review, Proceeding of IBS2003 Conference.*

Cerioni R, Doinda G (1994). A finite element model for the nonlinear analysis of reinforced and prestressed masonry wall. *Computer and Structures,* 53, 1291-1306.

Lotfi H, Shing P (1991). An appraisal of smeared crack model for masonry shear wall analysis. *Computer and Structures,* 41, 413-425.

Oh K (1994). Development and Investigation of Failure Mechanism of Interlocking Mortarless Block Masonry System. *Ph.D. thesis,* Drexel University, Philadelphia.

Riddington JR, Noam NF (1994). Finite element prediction of masonry compressive strength. *Computer and Structures*, 52(1), 113-119.

Suwalski P, Drysdale R (1986). Influence of slenderness on the capacity of concrete block walls. *Proceeding of 4th Canadian Masonry Symposium*, 122-135.

Zhuge Y, Thambiratnam D, Coreroy J (1998). Nonlinear dynamic analysis of unreinforced masonry. *ASCE's Journal of Structural Engineering*, 124(3), 270-277.

Challenge Journal of Structural Mechanics

Earthquake design of a viaduct with full seismic isolation of bridge deck

Martin Wieland [a,*], Sujan Malla [b]

[a] *Poyry Switzerland Ltd., Herostrasse 12, CH-8048 Zurich, Switzerland*
[b] *Axpo Power AG, Parkstrasse 23, CH-5401 Baden, Switzerland*

ABSTRACT

The Arachthos Bridge in Greece is about 1 km long and crosses the future Arachthos reservoir. This paper presents the results of the earthquake analysis of the bridge design that won an international design competition. The spans vary from 83 m to 107 m. The Y-shaped piers with heights of up to 80 m are founded on piles. Because of the high seismic stresses in the bridge piers, hydraulic dampers are needed in both the longitudinal and transverse directions. The dampers reduce the seismic stresses in the piers by about 50%. The optimisation of the seismic dampers is discussed in this paper. Two transverse seismic dampers are provided on each pier and one at each abutment. The seismic dampers allow relative movements between the bridge deck and the top of the bridge piers of up to ∓500 mm in the transverse direction. The longitudinal stability of the bridge girder under the static and dynamic loads is achieved by the piers, which are connected with the girder in the longitudinal direction, and the seismic dampers at the abutments. In the longitudinal direction, seismic movements of up to ∓250 mm are allowed. The longitudinal dampers at the ends of the bridge girder must allow both longitudinal and transverse movements. The dynamic analysis shows that maximum residual transverse movements of up to 200 mm are possible. Therefore, provision for the placement of hydraulic jacks is foreseen on the pier tops for re-centering the bridge deck after a strong earthquake. The stability of the bridge girder under the service loads is provided by shear keys, which are integrated in the pot bearings. Under the design earthquake or an earthquake exceeding the design earthquake, the bridge girder is prevented from falling down from the bearings.

ARTICLE INFO

Article history:
Received 23 January 2015
Accepted 21 March 2015

Keywords:
Earthquake
Continuous girder bridge
Base isolation
Seismic design
Dynamic analysis

1. Introduction

The Arachthos Bridge, which is a part of the Egnatia Motorway in Greece, is about 1 km long, straight in plan and slightly sloping in the longitudinal direction. The bridge crosses the future Arachthos reservoir. This paper presents the results of the earthquake analysis of the bridge design that won an international design competition, in which aesthetics played an important role. The length of the bridge and the small height of the visible part of the piers above the water level, after the filling of the reservoir, led the designers to select a very slender prismatic structure supported on three-dimensional "sculptural" piers.

The bridge is up to 80 m above the ground level and the distance between the piers varies from 83 to 107 m. This distance complies with the most economic span lengths, which amounts to approximately 70 meters for free cantilever construction. The Y-shaped piers are founded on piles. The superstructure is composed of a post-tensioned single-cell concrete hollow box with cantilevering deck slabs. The total width of the bridge deck is 28 m.

The cross-section of the deck was designed to look slender from far away, as well as to be constructed and maintained easily. Special emphasis was paid on shaping the elements of the bridge and their details. The criteria for the design of these elements were, in order of importance: (i) aesthetics and pleasing overall design as

* *Corresponding author*. Tel.: +41-76-3562862 ; Fax: +41-44-3555563 ; E-mail address: martin.wieland@poyry.com (M. Wieland)
ISSN: 2149-8024 / DOI: http://dx.doi.org/10.20528/cjsmec.2015.03.007

well as attention to detailing, (ii) the structural behaviour of the bridge, under static and dynamic loads, and (iii) a simple construction process and cost considerations. The bridge has a unique and efficient design, which also creates a landmark in the area.

2. Seismic Isolation System

Because of the relatively low stiffness of the bridge system in the longitudinal and transverse directions and the resulting high flexural and axial stresses in the bridge piers, seismic dampers are needed in both the longitudinal and transverse directions. By means of hydraulic dampers with a friction-type hysteresis loop, the seismic stresses in the piers can be reduced by approximately 50%.

The hydraulic dampers have the advantage that no damping force is produced by slow movements, i.e. changes in the bridge deck caused by shrinkage, creep and temperature effects do not cause any loads on the abutments. The technical and economical feasibility of the dampers has been discussed with specialized manufacturers of seismic dampers.

Seismic dampers with a total damping force of 21 MN shall be provided at each abutment in the longitudinal direction. Six dampers with a damping force of at least 3.5 MN shall be provided. In general, the dampers shall only transfer compressive loads towards the abutments and exert only a small tensile force (maximum 5% to 10% of the compressive forces). However, during the bridge construction, at least two dampers at the fixed support is need to be designed to transmit both tensile and compressive forces.

In the longitudinal direction, the maximum static movements are +200 mm/-300 mm and the maximum allowable seismic movements are ∓250 mm. The expansion joints at the ends of the bridge girder shall be able to cope with the static movements. As damage of the expansion joints may be accepted under the design earthquake, the seismic design criteria of the expansion joint, which is not a vital element of the bridge, may be relaxed in order to achieve an economical solution.

Two seismic dampers of the same type as for the longitudinal direction, with a damping force of 1 MN each, shall be provided in the transverse direction on each pier. In addition, one transverse damper of 1 MN is provided at each of the two abutments. The seismic dampers shall allow relative transverse sliding movements of the bridge deck with respect to the top of the bridge piers of up to ∓500 mm. This situation requires an increased sliding plate at the pot bearings. At the abutments, the maximum allowable transverse movement was taken as ∓300 mm.

In the design of the dampers, it shall be considered that the maximum static and dynamic movements do not occur at the same time. The dampers at the abutments must allow longitudinal and transverse movements. Hence, the seismic dampers in the longitudinal direction must be provided with spherical hinges in order to allow combined longitudinal and transverse movements at the ends of the bridge girder.

For the seismic monitoring, strong motion instruments (accelerometers) with event recording will be provided at the abutments and on selected piers.

The static and dynamic stability of the girder in the longitudinal direction is assured by means of the piers, which are connected with the bridge girder (piers P1 to P8) and the seismic dampers at the abutments. In order to stabilize the bridge deck in the transverse direction under transverse loads caused by wind, traffic, and small to moderate earthquakes, shear keys are provided with a predefined breaking force, which is almost equal to the damper force. The shear keys are integrated in the pot bearings. Under the design earthquake or an earthquake exceeding the design earthquake, the bridge girder is prevented from falling down from the bearings by the seismic dampers, i.e. the piston of the cylindrical damper touches the damper head.

3. Design Earthquakes

The peak ground accelerations of the design earthquake (embedment of pier foundations in rock) in horizontal and vertical directions are 0.16 g and 0.11 g respectively. In addition, an importance factor of 1.3 has to be taken into account for the seismic design of the bridge. The design earthquake motion is given in the form of an acceleration response spectrum for a damping ratio of 5%. The bridge has to be designed in such a way that no inelastic deformations occur in the structural elements of the bridge piers and the bridge girder under the design earthquake.

The peak ground acceleration of the earthquake action to be considered for the different construction stages of the bridge is 50% of that of the design earthquake, i.e. 0.08 g in horizontal direction and 0.056 g in vertical direction. This corresponds to an earthquake with an average return period of less than 100 years. In addition, the importance factor for the construction phase is taken as 1.0.

4. Specific Verifications

Specific verifications are required for the safety of the equipment on the bridge girder during construction under the wind and earthquake actions. For the seismic safety checks, the peak acceleration on the bridge deck, calculated for a structural model where the girder is fixed to the pier head, shall be used. As the eigenfrequencies of the equipment are much higher than those of the free-standing pier, it is sufficient to perform a pseudo-static analysis of the equipment.

To carry the horizontal wind and earthquake loads during the free cantilever construction of the bridge girder, the need for stabilizing of the piers by means of cables, which are connected to the corners of the pier head, has to be checked. If needed, the optimum layout of the stay cables has to be determined, and the corresponding anchor points must be provided on the ground. In view of the high mass of the bridge piers and the bridge girder, relatively high cable forces will result. The effect of the cable sag has to be taken into account in the analysis of the free-standing piers.

5. Analysis for Seismic Loads – Basic Assumptions

The basic assumptions of the structural modelling and dynamic analysis are as follows:

- The bridge deck and the piers are modelled using standard three-dimensional linear-elastic beam elements formulated on the basis of the Bernoulli-Euler beam theory, corrected for shear deformation effects. Each beam element has two nodes at the ends, and there are six degrees of freedom (i.e. three translations and three rotations) per node. (Fig. 1).

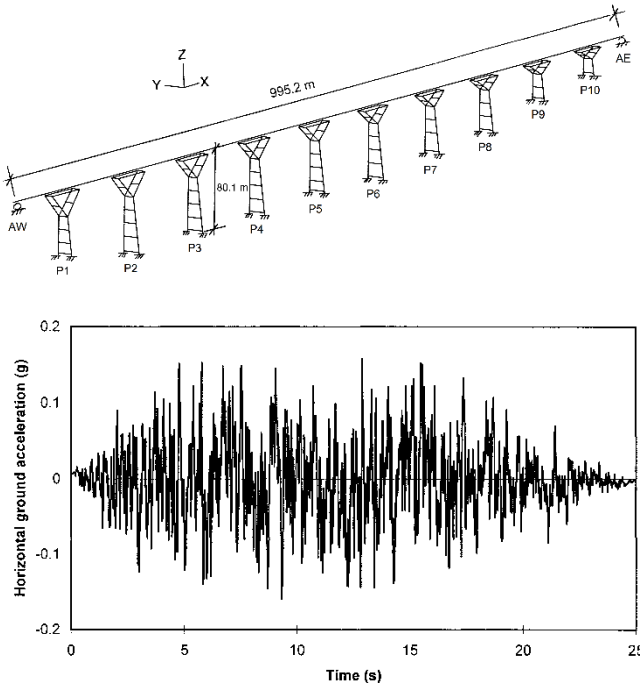

Fig. 1. Finite element model of Arachthos bridge and artificial accelerogram used for inelastic dynamic analysis.

- Strains, displacements and rotations are assumed to remain small.
- The dynamic modulus of elasticity of concrete is taken as 37 GPa.
- The effect of the water in the submerged portions of the piers is modelled by added masses.
- The mass of the 20% of the live (traffic) load has been considered in the dynamic model.
- All members, except the cross-beams in the piers, are assumed to be uncracked.
- The cracked flexural stiffness of the cross-beam section is assumed to be equal to 25% of the uncracked stiffness of the concrete section.
- The end zones of the main cross-beams of the piers are assumed to be rigid.
- All pier legs are assumed to be fixed at the base.
- At the abutments, the vertical displacement and the torsional rotation of the bridge are blocked.
- The longitudinal and transverse dampers are modelled as elasto-plastic elements. The damper forces of 2 MN in the transverse direction and 21 MN in the longitudinal direction include the effect of friction in the sliding bearings, which has the same hysteretic characteristics as the dampers.
- The bridge deck is supported vertically at four corners on the top of each pier. The deck can slide freely in the transverse direction at these bearings. Dampers control the transverse displacements of the bridge deck relative to the pier tops.
- The three components of the earthquake ground motion are represented by spectrum-compatible artificial accelerograms (Fig. 1).
- The ground motion is assumed to be uniform at all supports of the bridge.
- The Rayleigh damping model is used for the structural damping with 5% damping of the predominant structural modes.

The three-dimensional structural model used for the earthquake analysis comprises 991 nodes and 1172 elements. There are 5696 dynamic degrees of freedom in the structural model (Fig. 1). The earthquake response was computed by means of the computer program ADINA by direct integration with time steps of 0.01 s using the Newmark method.

6. Inelastic Seismic Analysis

An eigenfrequency analysis was carried out first to determine the eigenfrequencies and the modes of vibration of the bridge under small amplitude vibrations, i.e. when the shear keys in the pot bearings are still intact. This analysis allows the engineer to better understand the dynamic behaviour of the bridge and to determine the modes that mainly contribute to the dynamic response of the bridge under earthquake loads. Eigenfrequency analyses were also carried out for construction stages (Fig. 2).

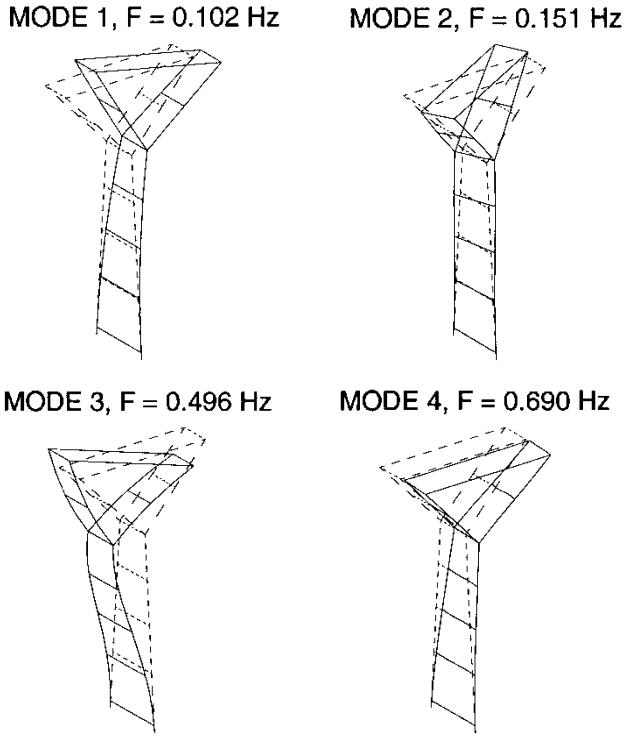

Fig. 2. Mode shapes and eigenfrequencies of highest free-standing pier during construction.

The seismic design was based on the results of inelastic earthquake analyses using eleven statistically independent sets of artificially-generated, spectrum-compatible earthquakes. Due to the non-linear behaviour of the seismic dampers, all seismic analyses have to be carried out in the time domain using a direct integration method (Figs. 3 to 5).

Non-linear analyses can be numerically quite sensitive; therefore, a number of numerical checks were necessary to confirm the reliability of the results. For the Arachthos Bridge, the following numerical checks were carried out:

- Reduction of time step from 0.02 s to 0.004 s
- Change of numerical integration method (Newmark method and Wilson-theta-method)
- Effect of error criterion (energy, displacement tolerance, etc.)
- Equilibrium iteration with Newton-Raphson method, etc.

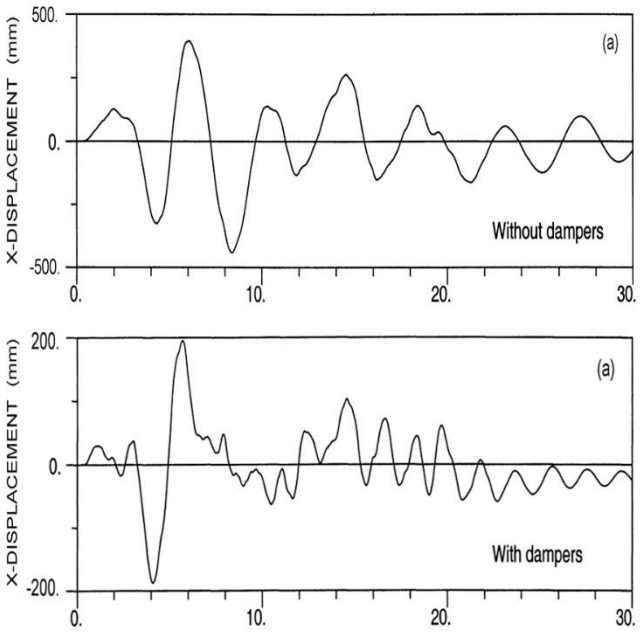

Fig. 3. Comparison of time histories of longitudinal displacement of bridge girder at abutment without (top) and with damper (bottom) (displacements in mm).

7. Design Considerations

In accordance with Eurocode 8 (2005), the results (bending and torsional moments, axial forces, shear forces, displacements, accelerations, relative movements of bearings and expansion joints, forces in dampers, etc.) of the eleven nonlinear earthquake analyses were averaged for the purpose of the seismic design of the bridge.

The bridge girder and the piers are designed to behave fully elastically under the design earthquake. Any damage will be confined to the pot bearings, where the shear keys will have to be replaced and the displaced bridge girder has to be moved to its original position by means of hydraulic jacks. In addition, local damage can be expected at the expansion joints. This seismic design concept will ensure that the bridge can be used safely during and after the design earthquake. The bridge is also expected to behave satisfactorily during an earthquake exceeding the design earthquake, as the design earthquake and the dynamic modelling of the bridge include a number of rather conservative assumptions, e.g. the uniform ground motion, which leads to an overestimate of the longitudinal and transverse movements of the bridge girder on the bearings.

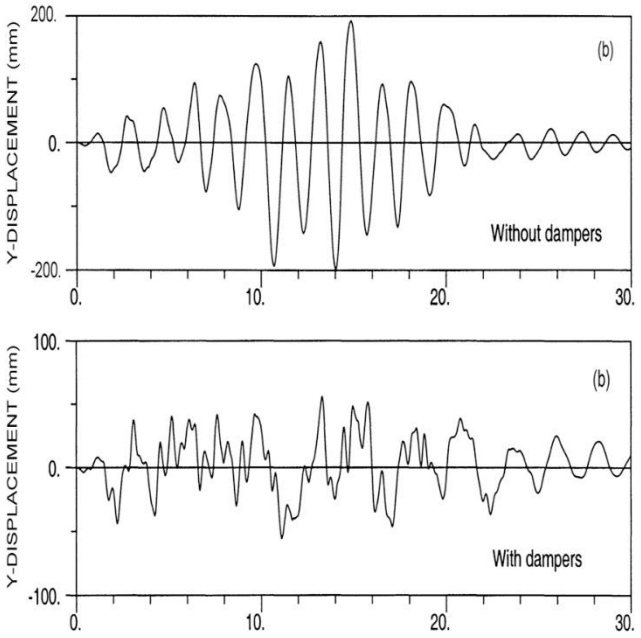

Fig. 4. Comparison of time histories of transverse displacement of top of highest pier without (top) and with damper (bottom) (displacements in mm).

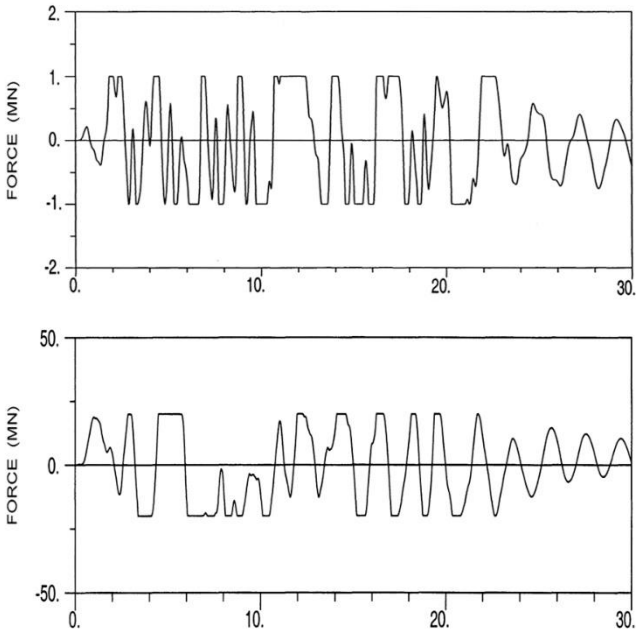

Fig. 5. Comparison of time histories of force in single transverse damper on highest pier (top) and total force in the longitudinal dampers at the abutment (bottom) (damper forces in MN).

8. Conclusions

By means of isolation of the bridge girder from the supports, the seismic forces can be greatly reduced in large continuous girder bridges susceptible to dynamic actions. The isolation is achieved by hydraulic dampers (other types of dampers may also be suitable), which are located at the bridge bearings.

In the case of the proposed Arachthos Bridge project, the seismic forces in the Y-shaped high piers with heights of up to 80 m could be reduced by about 50% as compared to the bridge without dampers. The maximum dynamic deflection of the pier heads transverse to the bridge axis could even be reduced by 75%. The maximum transverse and longitudinal sliding movements on the bearings due to the earthquake shaking were calculated as ∓40 cm and ∓24 cm, respectively, which are within the allowable limits.

Because of the nonlinear characteristics of the dampers with an almost rectangular hysteretic loop under the seismic action, extensive nonlinear dynamic analyses were carried out for the optimization of the dampers and for the calculation of the seismic design forces and deformations. It is obvious that seismic dampers do not only protect a bridge from large seismic forces but also result in a very economical solution, as modifications in the structural system of a bridge might be much more expensive than the installation of dampers. In the case of Arachthos, it was required that the bridge behaves elastically under the design earthquake, a requirement which is hard to fulfil with conventional design options. It must be added that the design response spectrum had very high spectral accelerations at low frequencies, which made the installation of dampers even more advantageous.

Instead of the winning bridge design, whose earthquake design is described in this paper, the owner decided to go for a more conventional bridge with a less challenging and aesthetic design.

References

Eurocode 8 (2005). Design of Structures for Earthquake Resistance. Part 2: Bridges, prEN 1998-2, European Committee for Standardization (CEN), Brussels.

Malla S, Wieland M (2003). Study on the dynamic behaviour of a base-isolated viaduct (in German), Current Status of Bridge Dynamics, SIA-Dokumentation D 0198, Zurich, Switzerland.

Challenge Journal of Structural Mechanics

Seismic behavior analysis of multi-story reinforced concrete buildings having torsional irregularity

Turgut Öztürk *, Zübeyde Öztürk, Onur Öztürk

Department of Civil Engineering, İstanbul Technical University, 34469 İstanbul, Turkey

ABSTRACT

Earthquakes are one of the most important and hazardous natural disasters in the world and in our country. They also have lots of characteristics from the point of effects caused by them. For this reason it requires special engineering approach to analyze those effects and to design earthquake resistant structures. Almost all of the life losses caused by the earthquakes are related with improperly designed buildings safety of which are not ensured against severe earthquakes. Structural damages and collapses cause very important economical losses. So, understanding of the characteristics of an earthquake and correct determination of the behavior of buildings under earthquake excitation turn out to be the most important requirement to build earthquake resistant buildings. When we take into consideration the destructive effects of severe earthquakes that happened especially in recent years (Kocaeli 1999, Düzce 1999) one can easily see the importance of knowing the behavior of buildings under earthquake loads. In this study torsional effects that occur during earthquake excitations are analyzed in multi-story reinforced concrete buildings. In that manner the behavior of reinforced concrete structures under earthquake loads are examined and by the way the behaviors of structures having torsional irregularities are enlightened and clarified. Moreover the effects of rigidity, ultimate capacity and ductility on the behavior of structures under ground motion are summarized. Torsional irregularity is a key irregularity in determination of the method to be used in earthquake analysis. Definition of the torsional irregularity of a multi-story reinforced concrete building is explained in accordance with Turkish Earthquake Code and the related principles of computations that have to be followed according to the code are given. Multi-story reinforced concrete buildings are classified according to their plan geometry and the effects of plan geometry on the torsional irregularity are explained. While in certain structures torsional irregularity may happen in very high levels in some structures it may happen so small that can be safely omitted. For that reason buildings forming torsional irregularity are classified and their characteristics and torsional irregularity parameters are given. Shear walls without causing any torsional irregularity on buildings having different plan geometries are shown.

ARTICLE INFO

Article history:
Received 28 January 2015
Accepted 22 March 2015

Keywords:
Earthquake
Seismic behavior
Multi-story building
Torsional irregularity
Building codes

1. Introduction

In this study, the torsional irregularity, which is one of the most important irregularities in seismic behavior, is examined. Among all irregularities, the torsional irregularity is taken into consideration at most in modern earthquake codes. In 39 of those earthquake codes, there are rules and regulations regarding to this irregularity. Some of regulations are;

- In 11 codes, the torsional irregularity is not allowed in any way. In 6 of them it is stated that seismic joints should be used.

* *Corresponding author*. Tel.: +90-212-2853842 ; Fax: +90-212-2853842 ; E-mail address: ozturkturg@itu.edu.tr (T. Öztürk)
ISSN: 2149-8024 / DOI: http://dx.doi.org/10.20528/cjsmec.2015.03.008

- In 3 codes, the application of additional eccentricity is stipulated.
- In 13 codes, it is stated that dynamic analysis and calculation should be applied.
- In 10 codes, it is stated that additional eccentricities should be increased providing that some certain conditions are fulfilled and in extreme cases it is stated that dynamic analysis and calculation should be utilized.

Generally the way of solution is; to increase the eccentricities then to repeat the lateral load analysis when parameters related with torsional irregularity exceed certain values and if there exists further increase of those parameters dynamic analysis should be applied. The same solution is also adopted in Turkish Earthquake Code, which came into operation on January 1st 1998 (Özmen, 2001).

2. Method of Analysis

In seismic analysis of the sample structure examined in this study; equivalent earthquake force method and mode superposition method are used. In both methods the floor masses are applied to the shifted story mass centers. Structure is analyzed under the assumption of the rigid diaphragm behavior of floor slabs. The spectrum diagram, which will be used in seismic analysis of the system, soil characteristics and earthquake zone parameters, are taken from Turkish Earthquake Code. In structural analysis, SAP2000 Structural Analysis Program is used. The torsional coefficients which are defined by Turkish Earthquake Code are calculated according to the equivalent earthquake force method then using the results obtained from that analysis additional eccentricities are given to the story mass centers and seismic analysis is repeated. As a result, the seismic analysis of the building is performed by; a) Equivalent earthquake force method at shifted mass center, b) Equivalent earthquake force method at shifted mass center with given additional eccentricity, c) Mode superposition method at shifted mass center.

3. Sample Structure

Because of the fact that the most serious torsional irregularities are seen on buildings having irregularity about the rigidity distribution, the sample structure is chosen geometrically regular. In this building the torsional irregularity is obtained by especially the assembly of shear walls closed to end edges i.e. the irregularity is obtained due to non-uniform rigidity distribution of vertical elements within the structure. What is aimed by choosing this sample is to emphasize that rather than the geometric characteristic of the building the load carrying system can also cause serious torsional effects. Consisting of 1 basement story, 1 ground story and 13 normal stories the building is a 15-story reinforced concrete structure. It has 28.50x19.00=541.50 m^2 living area which is rectangular in plan. At normal stories on 3 sides, projections having 1.5 m and 2 m span lengths are formed. Structural system of the building is formed with rectangular columns, polygon shaped shear walls and beams. The structural system is totally symmetrical in *y* direction but not in *x* direction. Total height of the building is 53.50m. Structural system is modeled as high ductility moment resisting frame system. Building is in the 2nd degree earthquake zone and Z2 local site class is assumed. Material types used in the project are C25 and S420. Floor plans a longitudinal section of the building are given in Figs. 1 and 2.

4. Classification of Buildings Having Torsional Irregularity

Buildings having torsional irregularity can be divided into 4 classes.
1. Buildings having geometrical irregularity.
2. Buildings having irregularity about rigidity distribution.
3. Buildings having irregularity about both geometry and rigidity distribution.
4. Buildings having hidden torsional irregularity.

5. Typical Buildings That Are Not Expected to Have Torsional Irregularity

A part of the results obtained from the studies done on buildings in this group are of expected type. However it is interesting to obtain some unexpected results. Some of the results are summarized below.
1. In general buildings that are symmetrical about both geometry and rigidity distribution have no torsional irregularity.
2. Buildings having shear walls especially on edges behave more regular about torsional irregularity.
3. In some buildings which are symmetrical about both geometry and rigidity distribution the torsional irregularity coefficients may approach to a limit value of 1.20.
4. It is concluded that for the torsional irregularity point of view the rigidity distribution is a more important factor than geometry.

6. Geometrically Irregular Buildings

Following results are obtained at the end of analyses performed on buildings belonging to this group.
1. Torsional irregularities of buildings having only geometric irregularity are not at very high levels. Even for buildings, which are unfavorable about torsion, torsional irregularity coefficients are at about 1.4.
2. In that type of buildings, small increases on sectional dimensions of elements along weak axes result in considerable decrease in torsional irregularity.
3. In unsymmetrical buildings, torsional irregularity coefficients stay at acceptable levels if there is no big irregularity about rigidity.

7. Irregular Buildings About Rigidity Distribution

At the end of analyses performed on buildings having rigidity irregularity following results are obtained.
1. In buildings having rigidity irregularity, the torsional can be at very high levels.

2. Even for buildings, which are unfavorable about torsion, the torsional irregularity coefficients stay below 2, which is the limiting value for the application of equivalent earthquake force given in Turkish Earthquake Code. So it can be clearly understood that it is nearly impossible to reach that value in structural applications.
3. Torsional irregularity can mostly be removed in this kind of buildings with arrangements done on load carrying elements along the weak axes of the structure.
4. The most effective way of decreasing the torsional irregularity is to locate the shear walls along the weak axes.
5. Increasing beam and/or column cross sectional areas can also be helpful for decreasing torsional irregularity in weak axes.
6. Even at the buildings having high amount of torsional irregularity, modeling difficulties may not be seen. It is brought forward that precautions in codes torsional irregularities need some change

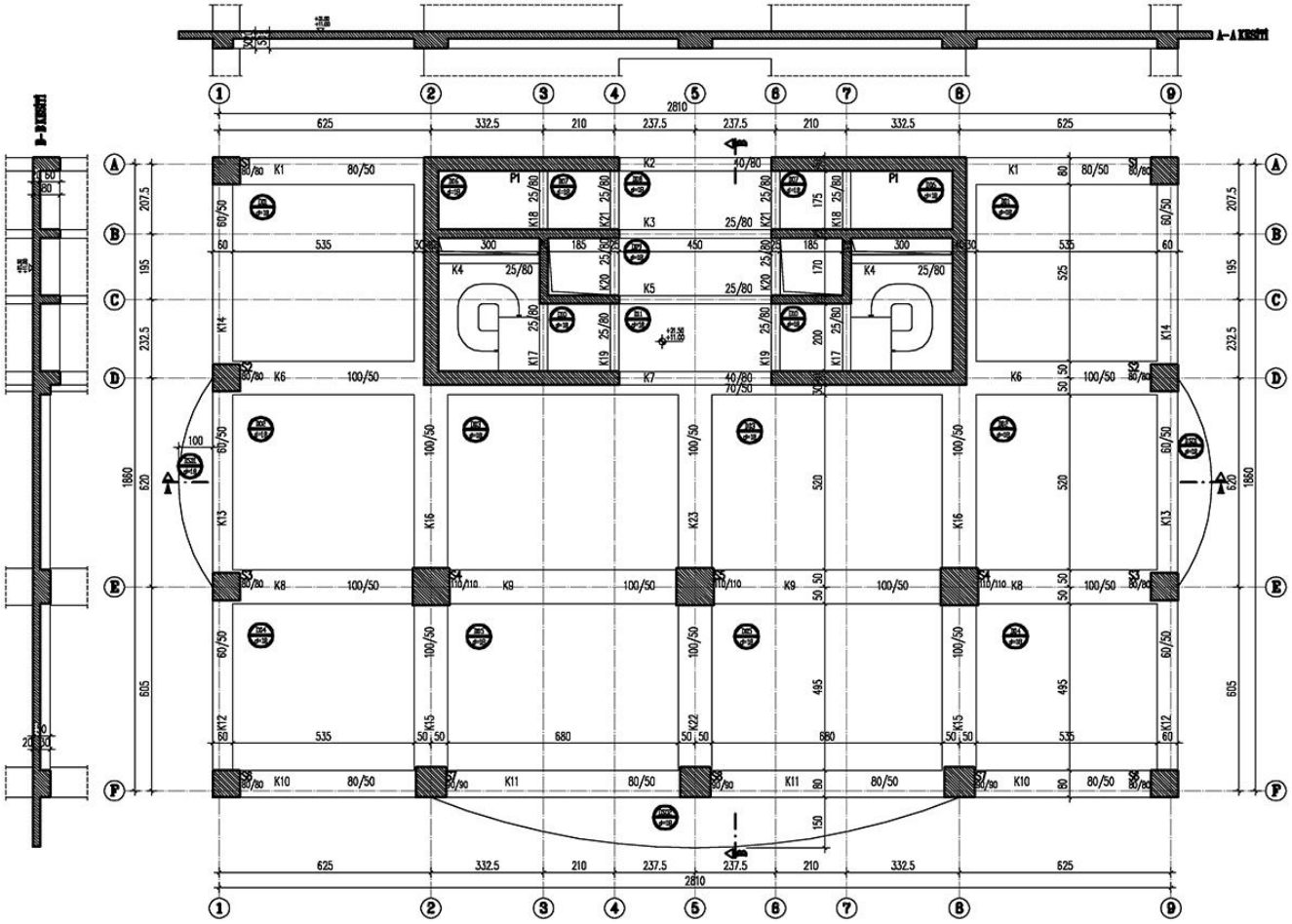

Fig. 1. Normal story formwork plan of the sample structure.

8. Irregularities in Geometry and Rigidity

The results obtained from studies done investigations on buildings in these groups are parallel to behavior occurred in "buildings having rigidity irregularity". The results are summarized below.
1. Torsional irregularity can be at high levels.
2. The torsional irregularity coefficients stay below the limiting value of 2.00 even at the buildings, which are unfavorable about torsion.
3. The torsional irregularity can mostly be removed with arrangements done on structural elements along weak axes of structure.
4. The most effective solution for decreasing the torsional irregularity is to locate the shear walls along the weak axes.
5. Even at the buildings having high amount of torsional irregularities, modeling difficulties may not be seen.

The behavior type of this type of building is parallel with irregular buildings only in aspect of rigidity distribution. Hence, it can be concluded torsional irregularity depends on almost only unbalanced rigidity distribution in the plan.

9. Hidden Torsional Irregularities

Following results are obtained at the end of analyses performed on building belonging to this group.
1. Torsional irregularity can also occur in the buildings having regular geometrical shape and regular rigidity.
2. The reason for torsional irregularity in this type of buildings is lack of rigidity on the edge axes.
3. Rigidity of edge axes must be increased in order to remove torsional irregularities.
4. In certain cases, torsional irregularity can be lowered or totally removed as a result of decrease in shear wall rigidity at the central zone (Özmen, 2001).

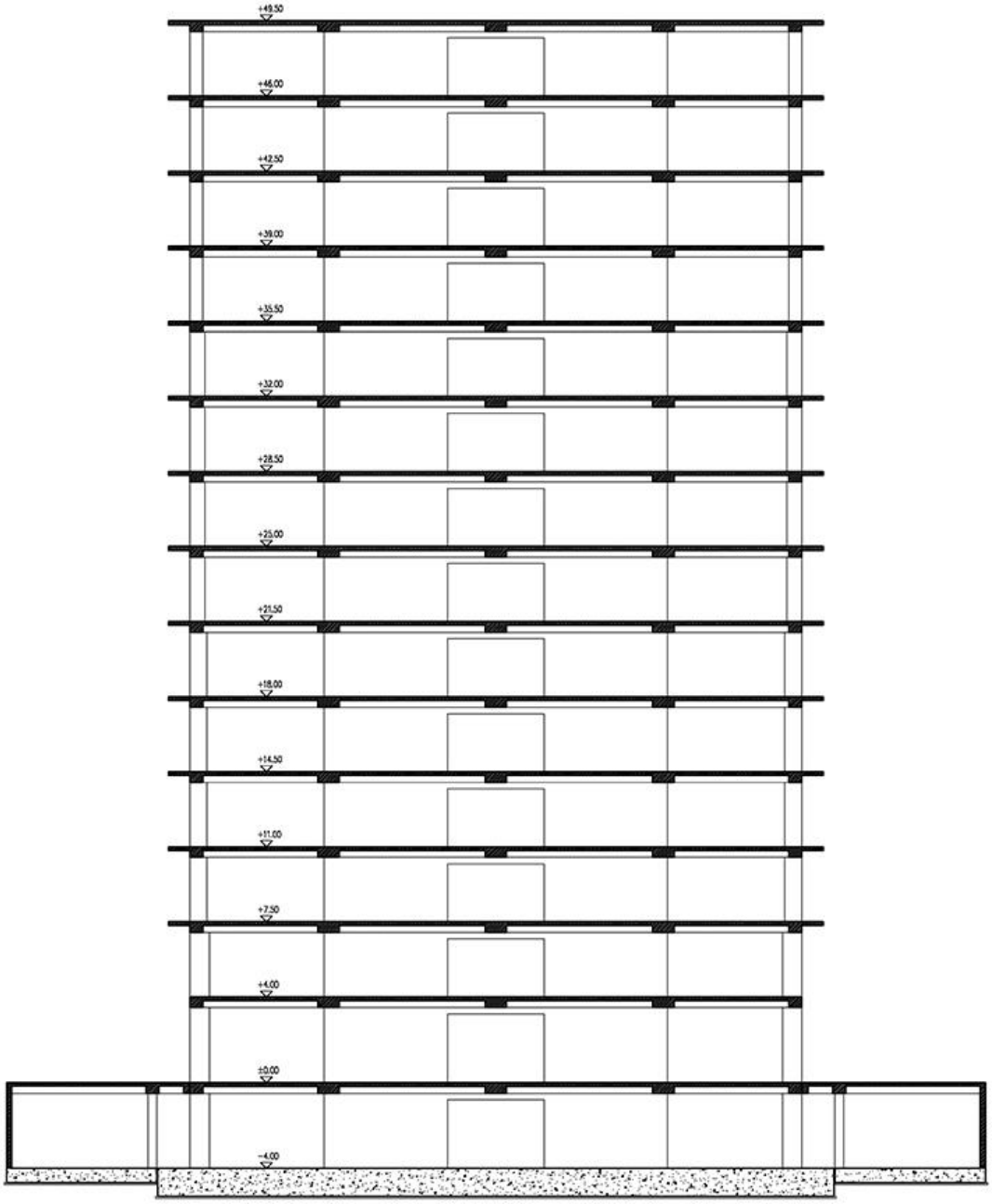

Fig. 2. Longitudinal section of the sample structure along *x* direction.

10. Analysis Results

As a result of analyses equivalent seismic load method and mode superposition method, torsional irregularity coefficient which are calculating according to relative and absolute story drifts are shown in Table 1 and Table 2.

Although it is geometrically symmetric, there occurs torsional irregularity in the building, because the rigidity distribution of the structural system is irregular. At the end of calculation, torsional irregularity coefficient for the building has been found as max η_b=1.529. It has been seen that the torsional irregularity is increases when the shear walls taking part on the sample building are located to outer axes. With the aid of this examination it can be concluded that torsional irregularity may be on very high levels on buildings, which are irregular from the viewpoint of rigidity distribution.

All these results clearly exposes the need of giving importance on the selection process of structural system. Structural systems begins to come out at the architectural plan phase. Often various architectural reasons do not allow modeling of the desired structural system.

However with some changes and additions that will not affect architectural made by the engineer on the forming phase of the structural system, torsional irregularity can be reduced to minimum levels. In the sample structure locating structural walls to symmetric axes where rigidity distribution is dense will be a precaution which will fairly decrease the degree of torsional irregularity.

On this kind of buildings, in order to reduce the degree of torsional irregularity, shear walls, even at a limited number and on a limited dimension have to be located to weak axes.

Table 1. Torsional irregularity coefficients calculated with equivalent seismic load method.

STORY	$X_{+0.05}$		$X_{-0.05}$		$Y_{+0.05}$	
	Relative η_{bi}	Absolute η_{bi}	Relative η_{bi}	Absolute η_{bi}	Relative η_{bi}	Absolute η_{bi}
1	1.385	1.385	1.529	1.529	1.170	1.170
2	1.362	1.370	1.499	1.509	1.159	1.162
3	1.326	1.351	1.460	1.489	1.146	1.155
4	1.311	1.339	1.443	1.474	1.138	1.150
5	1.297	1.328	1.427	1.462	1.131	1.145
6	1.286	1.319	1.416	1.452	1.125	1.140
7	1.276	1.312	1.405	1.444	1.120	1.137
8	1.276	1.306	1.404	1.438	1.116	1.133
9	1.267	1.301	1.395	1.433	1.111	1.130
10	1.260	1.297	1.387	1.428	1.106	1.127
11	1.251	1.293	1.377	1.423	1.100	1.124
12	1.248	1.289	1.375	1.419	1.096	1.122
13	1.234	1.285	1.359	1.415	1.090	1.119
14	1.219	1.281	1.343	1.411	1.084	1.116
15	1.196	1.277	1.317	1.406	1.078	1.114

Table 2. Torsional irregularity coefficients calculated with mode superposition method.

STORY	$X_{+0.05}$		$X_{-0.05}$		$Y_{+0.05}$	
	Relative η_{bi}	Absolute η_{bi}	Relative η_{bi}	Absolute η_{bi}	Relative η_{bi}	Absolute η_{bi}
1	1.411	1.411	1.491	1.491	1.223	1.223
2	1.385	1.394	1.465	1.474	1.222	1.222
3	1.346	1.374	1.427	1.455	1.218	1.220
4	1.327	1.359	1.407	1.440	1.223	1.217
5	1.308	1.347	1.388	1.427	1.225	1.219
6	1.294	1.336	1.372	1.416	1.226	1.220
7	1.282	1.327	1.359	1.407	1.223	1.221
8	1.279	1.320	1.356	1.400	1.219	1.220
9	1.269	1.314	1.345	1.393	1.211	1.219
10	1.261	1.309	1.338	1.388	1.201	1.217
11	1.251	1.304	1.329	1.383	1.189	1.214
12	1.247	1.299	1.327	1.378	1.177	1.211
13	1.231	1.295	1.312	1.374	1.163	1.207
14	1.213	1.290	1.294	1.370	1.150	1.203
15	1.185	1.285	1.266	1.365	1.138	1.199

As a result of analyses explained in the above paragraph and the result of researches made on this subject, it has been determined that only on the geometrically irregular buildings torsional irregularity is not on high-levels. Begin on very high-levels of torsional irregularity for buildings having H, L, T and Y shapes on the plans, is related with the rigidity distribution of the structural system. At the end of the little dimension increases on the structural elements on the weak axes of these kind of buildings, torsional irregularity can be removed on a large scale.

Obtaining max η_b=1.529 in the examined building and in the frame of made researches even on inconvenient buildings from the viewpoint of torsibility, η_b torsional irregularity coefficients remained under value 2.0 which has been determined as limiting value for applying equivalent load seismic method in Turkish Earthquake Code. On the application, meeting boundary value appears to be an impossible subject.

In the *y* direction, the building which is entirely symmetrical in the vertical direction, results in torsional irregularity coefficient η_b=1.170. Also with the dynamic

analyze, it is resulted in η_b=1.226. The values nearly become with the boundary value, shown in Turkish Earthquake Code for the obtaining the irregularity of the buildings, show that the irregularity coefficient is not realistic. It can be evaluated that considering the earthquake effects of 5% additional eccentricities results in the torsional irregularity coefficient of the *y* direction becomes nearly to 1.20 where the building is entirely symmetrical in the vertical direction.

Additional eccentricities had been found 8.12% with the aid of calculated torsional irregularity and then the analysis reviewed with the new eccentricity. The analyze show that additional eccentricity make frame end forces 1.4% much bigger in columns and beams, 2-4% much bigger in shear walls than with the 5% eccentricity. Modeling difficulties hadn't been encountered after these analyze results. For this reason, reviewing the analysis with the additional eccentricity, which is located as a precaution for the torsional irregularity in Turkish Earthquake Code, cause suspicion whether it is necessary or not.

The comparison between the frame end forces calculated by Superposition of Modes Method under dynamic analyze and Equivalent Load Method has given following results.

- The modal analyze results are much more inconvenient in the beam far away from the zone where buildings rigidity dense. However equivalent seismic loads results are much more inconvenient in the beam in zone where rigidity is dense.
- The equivalent earthquake loads results in columns close to axis passing through buildings mass center are; frame end forces in earthquake direction much more inconvenient whereas in the column far away from these axes the frame end forces in modal analyze results is inconvenient.
- The equivalent earthquake loads results in structural walls near to the mass center are; frame end forces in earthquake direction much more inconvenient whereas in the shear walls far away from mass center the frame end forces in modal analyze results is inconvenient.

The important result is, frame end forces and modal analyze results occurred by the orthogonal to the earthquake direction are much bigger than the equivalent earthquake load results. This situation is explained as that the torsional irregularity resulting from earthquake loads identified more realistically by dynamic analyze. Although the major frame end forces are much bigger than the minor frame end forces, there hadn't been observed any effect for modeling.

The maximum irregularity coefficient is found η_b=1.529 when the absolute displacements are used. However the reason of the equality of this value and torsional irregularity coefficients which are calculated by the relative displacements is that the maximum value occurs in the basement floor. However, using the absolute or relative displacements in order to find out irregularity coefficient, does not affect the results. (2nd floor η_b=1.509; relative η_b=1.499).

11. Conclusions

Torsional irregularity can occur in the buildings that have regular geometrical shape and regular rigidity distribution. The reason of this irregularity which is called hidden torsional irregularity, is due to lack of rigidity along the extern axes. In certain cases, torsional irregularity can be lowered or totally removed as a result of decrease shear wall rigidity at central zone.

As a conclusion torsional irregularity is more related to the rigidity distribution than the geometrical plan of the building. For this reason, determination of the load carrying system of a structure is the most important issue at the planning stage of the project. It is essential that shear wall locations and cross-sectional areas must be properly selected, and the shear walls must be symmetrical in the plan in order to prevent torsional irregularity. Today, availability of the computer software makes the solutions more precise. The important issue at this subject is whether the load carrying system is appropriate to the behavior manner of the structure or not. However, it must not be forgotten that the behavior of the structure does not work always as expected. It should be known that planning and design stage is not composed only of structural analyze and sectional calculations.

References

Eurocode 8 (1998). Design Provisions for Earthquake Resistance of Structures. Commission of the European Communities, European Committee for Standardization.

Özmen G (2001). Torsional irregularity in multi-story structures. *Turkey Earthquake Foundation, Technical Report*. TDV/TR 036-61. İstanbul, Turkey.

Özmen G, Pala S, Gülay G, Orakdöğen E (1998). Effect of structural irregularities to earthquake analysis of multi-story structures. *Turkey Earthquake Foundation, Technical Report*. TDV/TR 027-28, İstanbul, Turkey.

Sap2000 (1997). Integrated Finite Element Analysis and Design Structures. Computer and Structures, Inc., Berkeley, California, USA.

Specification for Structures to be Build in Disaster Areas (1998). Ministry of Public Works and Settlement Government of Republic of Turkey. Ankara, Turkey.

Uniform Building Code (1997). International Conference of Building Officials. California, USA.

Wilson EL (1998). Three Dimensional Static and Dynamic Analysis of Structures. Computer and Structures, Inc., Berkeley, California, USA.

Challenge Journal of Structural Mechanics

Dynamic response property of cooling tower structures

Takashi Hara *

Department of Civil Engineering and Architecture, Tokuyama College of Technology, 3538 Kume Takajo, 745-8585 Shunan, Japan

ABSTRACT

Reinforced concrete (R/C) cooling tower structures have been used for cooling down the hot water produced by power or chemical plants. These structures are designed to prevent against the failure under a self-weight and a wind loading, as well as an earthquake loading. In this paper, the numerical scheme under parallel processing is introduced and the dynamic evaluation of the cooling tower under an earthquake loading is examined. In numerical analyses, the cooling tower is assumed to have two types of conventional column system, i.e., V-column and I-column systems. Both R/C shell portion and column system are modeled by use of solid elements. From the numerical analyses, the higher stress concentrations are arisen between the junctions of R/C shell and columns for I-column than those for V-column. Also, it is concluded that the additional reinforcements should be placed around the junction considering the seismic effects.

ARTICLE INFO

Article history:
Received 28 January 2015
Accepted 23 March 2015

Keywords:
Cooling tower
R/C shell
Column support
Finite element method
Parallel processing
Dynamic response

1. Introduction

Reinforced concrete (R/C) cooling tower structures have been used for cooling down the hot water produced by power or chemical plants. These structures are designed to prevent against the failure under a self-weight and a wind loading, as well as an earthquake loading. To grow up the economy of developing countries, these structures may be built around the strong seismic regions due to supply the electric energy. Therefore, engineers must examine the safety of a cooling tower under earthquake loading. However, these structures are constructed with a large surface of R/C shell and columns and the numerical analyses are laborious and difficult based on the conventional numerical analyses.

To overcome these problems, several numerical schemes have been proposed combining the axisymmetric analyses or modal analyses (Hara and Gould, 2002; Lang et al., 2003). However, it is difficult to represent the local behavior of these structures by such numerical scheme. Although the finite element method (FEM) is one of the useful schemes, there must be a numerical effort to apply FEM to such problems, especially under a dynamic loading.

In this paper, the numerical scheme under parallel processing is introduced (Adeli and Soegiarso, 1999) and the dynamic evaluation of the cooling tower under an earthquake loading is performed. The parallel processing to compute the behavior of the cooling tower structure was proposed by Hara and the numerical efficiency was presented (Hara, 2004a). In this paper, the cooling tower is assumed to have two types of conventional column system, i.e., V-column and I-column systems. Examples of the column supported cooling towers are shown in Fig. 1.

In numerical analyses, R/C shell portion and column system are modeled by use of solid elements because the smooth combination of the deformations and the stresses between columns and R/C shell portion. Also, the EBE approach to the huge R/C structures is applied. Then the deformation characteristics of R/C shell with supporting columns are examined.

2. Numerical Scheme

2.1. Definition of the solid element

The 20 noded solid elements are adopted to model both shell and column portions. R/C shell elements are composed of the concrete and the reinforcing materials. To define the concrete nonlinearity, Drucker-Prager

* *Corresponding author*. Tel.: +81-834-29-6325 ; Fax: +81-834-29-6325 ; E-mail address: t-hara@tokuyama.ac.jp (T. Hara)
ISSN: 2149-8024 / DOI: http://dx.doi.org/10.20528/cjsmec.2015.03.009

yield criterion and Madrid parabola is used to trace the nonlinear stress strain relation of concrete. Also, the maximum principal tensile crack criterion is used to define the occurrence of the initial cracks. Tension stiffening and the stress degradation after cracks of concrete are adopted. In addition, reinforcing steels are modeled as the equivalent sheet with stiffness only of bar direction. The detailed definition is represented in the previous paper (Hara, 1988; Hara, 2004a; Hara, 2006).

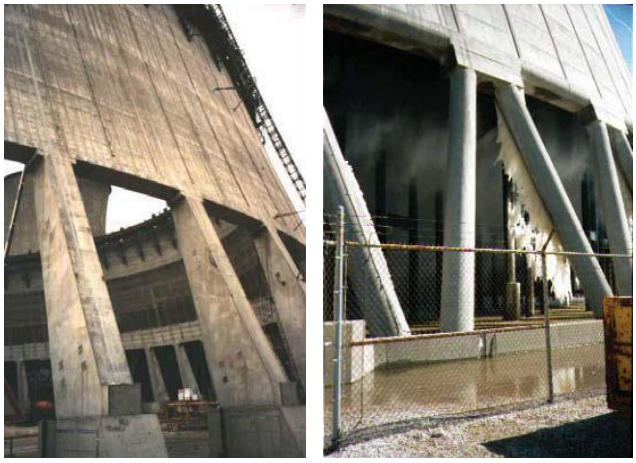

I-column V-column

Fig. 1. Cooling tower column systems.

2.2. Dynamic response analysis

During the time increment, the dynamic equilibrium equation is represented as follows:

$$M\Delta\ddot{y} + C\Delta\dot{y} + K\Delta y = -MI\Delta\ddot{y}_0 \,, \tag{1}$$

where M is the mass matrix, C is the damping matrix, K is the stiffness matrix. Δy, $\Delta\dot{y}$ and $\Delta\ddot{y}$ are the response displacement, the response velocity and the response acceleration vector, respectively. $\Delta\ddot{y}_0$ is the ground motion acceleration and Δ denotes the increment. In this analysis, Raileigh damping is adopted to define the damping matrix. To solve Eq. (1), the Newmark method is adopted in this paper. Then, the dynamic equiliburium equation systems, Eq. (1), is transformed as follows:

$$\tilde{K}y = \tilde{f} \,, \tag{2}$$

where

$$\tilde{K} = \frac{M}{\beta\Delta t^2} + \frac{C}{2\beta\Delta t} + K \quad \text{and}$$

$$\tilde{f} = -MI\Delta\ddot{y}_0 + M\left(\frac{\Delta\dot{y}}{\beta\Delta t} + \frac{\Delta\ddot{y}}{2\beta}\right) + C\left\{\frac{\Delta\dot{y}}{2\beta} + \left(\frac{1}{4\beta} - 1\right)\Delta y\Delta t\right\} \tag{3}$$

are the effective stiffness matrix and the modified load vectors, respectively.

In this paper, the dynamic response is evaluated with a time step of Δt=0.001sec. The damping factor is considered 3% proportional to the mass by Rayleigh damping. The convergence rule of equation of motion is defined by Newton-Raphson method

2.3. EBE procedure

To solve the dynamic response of structure, element-by-element (EBE) solution techniques (Hughes et al., 1983) are applied to Eq. (2). Each term of Eq. (2) is assembled by each element equilibrium equations. Then the equation is solved by use of the conjugate gradient method (Adeli and Soegiarso, 1999). PC cluster is applied to solve Eq. (2). In this analysis, PC cluster is composed of eight personal computers and a switching hub to connect each other. The data communication of each computer is governed by MPI.

In conjugate gradient scheme, the solution vector y_{k+1} and the gradient vector r_{k+1} are represented as follows:

$$y_{k+1} = y_k - \alpha_k p_k \quad , \quad r_{k+1} = r_k - \alpha_k \tilde{K} p_k \,, \tag{4}$$

where

$$\alpha_k = \frac{r_k^T r_k}{p_k^T \tilde{K} p_k} \quad , \quad p_{k+1} = r_k + \beta_{k+1} p_k \quad , \quad \beta_{k+1} = \frac{r_{k+1}^T r_{k+1}}{r_k^T r_k} \,. \tag{5}$$

In Eq. (5), $\tilde{K}p_k$ is calculated by element by element. Therefore, these are easy to parallelize.

3. Numerical Model

Fig. 2 shows the numerical models of the R/C cooling tower. The model is a half of R/C shell considering the symmetry of the configuration, the loading and supporting conditions. Both models are divided into 32 elements in hoop direction and into 30 elements in meridional direction. The height is about 175 m. The thickness of the shell changes 105 cm at the lintel through 20 cm at the top. In R/C shell structure, reinforcements are doubly placed in both hoop and meridional direction. The reinforcing ratio is 0.2%. On the other hand, reinforcements are placed 2% in the columns. R/C hyperbolic shell is supported on the 16 columns. Each column has 90 cm square cross section and 9.17 m length. In I-column model, the supporting columns are placed equidistance. In V-column model, the supporting columns are placed equidistance and the adjacent top of the columns are connected. Each column is divided into four elements to represent the flexural deformation of the columns. The material properties are shown in Table 1. The geometric properties are shown in the previous papers in detail (Hara, 2004a; Hara, 2006).

4. Dynamic Response of Cooling Tower with Column

4.1. Deformation behavior of R/C cooling tower shell

To evaluate the basic dynamic response properties of R/C cooling tower, the step load of 0.1g (g: gravity acceleration 980 cm/s^2) is applied. From the numerical analysis, the natural frequencies of the shell response with I-columns are 1.05 Hz and 2.70 Hz from the lintel and the

top response, respectively. They show different responses. In the case of the shell without columns, the natural frequency of this model shows 3.5 Hz (Hara, 2004b).

In the case of the shell with V-columns shows the natural frequency of 2.66 Hz. The amplitudes of the displacements on both lintel and the top are different. But the natural frequencies of them are the same.

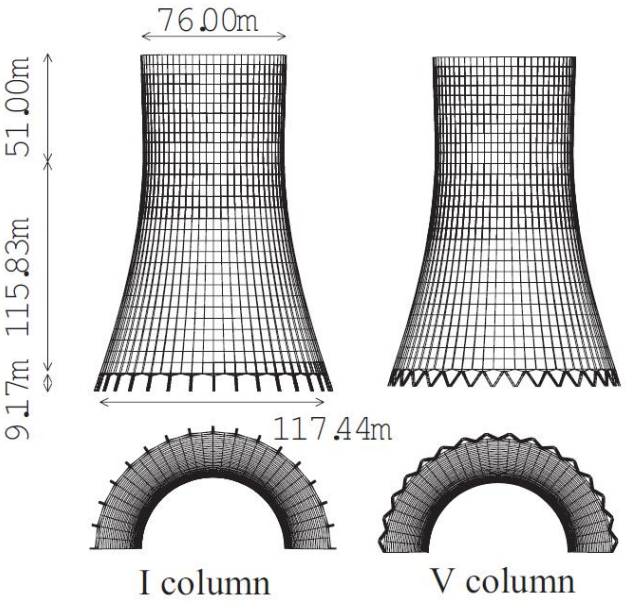

Fig. 2. Numerical models.

Table 1. Material properties.

Concrete	
Elastic Modulus	34 GPa
Poisson's Ratio	0.167
Density	0.0023 kg/cm^3
Compressive Strength	36 MPa
Tensile Strength	2.7 MPa
Reinforcing steel	
Elastic Modulus	206 GPa
Tangent Modulus	2.1 GPa
Yield Stress	500 MPa

Figs. 3 and 4 show the deformation patterns of R/C cooling tower with I-columns and V-columns, respectively. The deformation of the shell with I-column represents the kink at the connection between the shell and the columns and the shell shows the rigid body rotation. On the other hand, the response of R/C cooling tower with V-column deforms like as the cantilevered column.

4.2. R/C cooling tower under harmonic loading

Figs. 5 and 6 show the responses of the cooling tower with I-columns and V-columns under the harmonic loading, respectively. The dotted and the solid line denote the response at the top and the lintel, respectively. In this analysis, the intensity of the load is 0.1g.

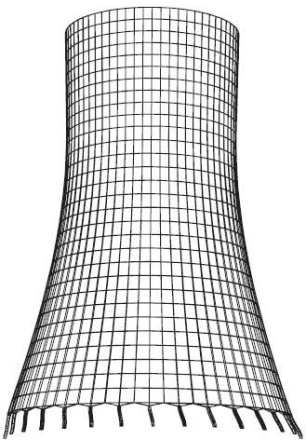

Fig. 3. Deformation under step load (I-column).

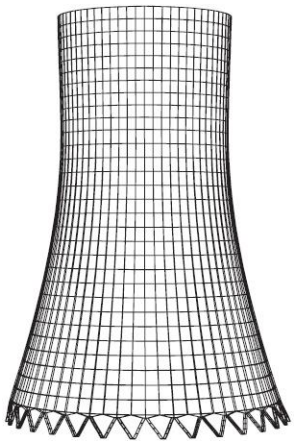

Fig. 4. Deformation under step load (V-column).

Frequencies of an external harmonic load are 1.05 Hz for the shell with I-columns and 2.66 Hz for the shell with V-columns, respectively. Fig. 5 shows the resonance response of the structure. In the case of I-columns, the large deformation is detected around the conjunction between the lintel and columns. Fig. 6 does not show the resonance response of the structure within 3 seconds. The cooling tower shell with V-columns shows the same deformation mode as that shown under step loading.

4.3. Effectiveness of parallel computing

Fig. 7 shows the relation between the numbers of processors and computing time. The calculation example is the response of the shell with I-columns under step loading. The greater the numbers of processors is, the fewer the computation time. However, these relations are not proportional because the computation time includes the process of the message passing.

5. Conclusions

This paper presented the numerical analysis of R/C cooling tower with column support under dynamic loading. To apply the general finite element to solve the huge R/C structure, the parallel computing technique is adopted.

From the numerical investigations, following conclusions are obtained.

- R/C cooling tower with I-column supports under dynamic loading shows local deformation around the junction between the lintel and columns but shows small deformation or distortion on the shell.
- R/C cooling tower with V-column supports under dynamic loading shows the cantilever type global deformation but the deformation is small.
- Total structural responses of the shell with supporting columns are different from the conventional pin-supported ideal shell (Hara, 2004b). Therefore, the precise total analyses must be considered.
- The numerical scheme presented here will be applicable to the practical one such as the earthquake response of the structure or the response of the dynamic wind loading considering the local deviations such as supporting columns and the hole on the shell surface.

REFERENCES

Adeli H, Soegiarso R (1999). High-Performance Computing in Structural Engineering. CRC Press.

Hara T (2004a). Dynamic response analysis of R/C cooling tower shell. *Proceedings of the WCCM VI in Conjunction with APCOM'04, Sep. 5-10,* Beijing, China.

Hara T (2004b). Dynamic analysis of R/C cooling tower shells under earthquake loading. *5th International Symposium on Natural-Draught Cooling Towers,* 283-291.

Hara T (2006). Dynamic response of R/C cooling tower shell considering supporting systems. *The International Symposium on Management Systems for Disaster Prevention ISMD.*

Hara T, Gould PL (2002). Local-global analysis of cooling tower with cutouts. *Computers and Structures*, 80, 2157-2166.

Hinton E (1988). Numerical Methods and Software for Dynamic Analysis of Plates and Shells. Pineridge Press, Swansea, U.K.

Hughes TJR, Levit I, Winget J (1983). An element-by-element solution algorithm for problems of structural and solid mechanics. *Computer Methods in Applied Mechanics and Engineering,* 36, 241-254.

Lang C, Meiswinkel R, Wittek U (2003). Anwendung von Schalenringelementen zur nichtlinearren dynamischen Berechnung von Stahlbeton-Rotationsschalen. *Beton- und Stahlbetonbau*, 98, 123-134.